Strategies for Dendrite-free Lithium & Sodium Metal Anodes

by

Ashok Sreekumar Menon

in partial fulfillment of the requirements for the degree of

Master of Science
in Material Science & Engineering

at the Delft University of Technology,
to be defended publicly on Wednesday July 12, 2017 at 02:00 PM.

Student number:	4449525	
Project duration:	October 2016 – June 2017	
Supervisor:	Prof. dr. Fokko M. Mulder	
Thesis committee:	Prof. dr. Fokko M. Mulder,	TU Delft
	Prof. dr. Andreas Schmidt-Ott,	TU Delft
	Dr. Amarante J. Böttger,	TU Delft
Daily Supervisor:	Ir. Yaolin Xu	TU Delft
Supervisors at TNO-Holst Centre :	Dorothee Hermes,	TNO, Eindhoven
	Dr. Lucas Haverkate,	TNO, Eindhoven
	Dr. Sandeep Unnikrishnan,	TNO, Eindhoven

This thesis is confidential and cannot be made public until December 31, 2018.

TU Delft Delft University of Technology

Industrial collaboration

This M.Sc graduation project was done under a collaboration between Prof. dr. F.M.Mulder (MECS group), Faculty of Applied Sciences and the High performance batteries group in TNO-Holst Centre, Eindhoven.

The Holst Centre is an independent research and development company in Eindhoven that was set up in 2005. It is a joint effort between TNO (Netherlands) and IMEC (Belgium). The main research focus of the company are sensor technologies, flexible and wearable electronics. The company is looking to diversify into other fields like high performance batteries.

Acknowledgements

This thesis project was carried out in TU Delft and the TNO-Holst Centre, Eindhoven. A lot of people at both places have been instrumental in helping me to complete this project.

Yaolin Xu, my daily supervisor for this work, has been the ideal guide I could have hoped for. He was patient and supportive throughout my work and was actively involved in moulding me as a researcher. I must admit that his enthusiasm has been the sole reason that I could complete this work on time. I'll forever be indebted to him for helping me produce a good master thesis work (and a possible publication).

Both my supervisors at TU Delft, Prof. Mulder and Prof. Böttger has been a constant source of support throughout the work. The good people working at the Storage of Electrochemical Energy section at the Reactor Institute in Delft has given me a comfortable environment to work in and an enjoyable time at the labs. I want to specially thank Frans G. Ooms and Michel Steenvorden who have helped me immensely throughout the work and sorted out a lot of problems (including some which were my fault). Peter-Paul Harks has also been a constant source of help and some of his inputs have been very useful in completing the thesis. Bernhard Weninger, Herman Schreuders and Joost Middelkoop (Materials for Energy Conversion and Storage group) at the applied science department was involved in helping me to setup the equipment and offered me guidance throughout the work. Jorrit Kroes, fellow master student, has also helped me with some experiments.

I also have to thank the people at Holst Centre as well. Dorothee Hermes has been a huge a support since the beginning of my project and helped me thoroughly to get this project up and running. Lucas Haverkate, Sandeep Unnikrishnan, Reza Fathi and Ellis Balder, other members of the battery group has played a big role is helping me complete this work. I want to specially thank Yann Petit, now a PhD candidate at TU Graz, for helping me significantly with the electrochemistry part and for some fun times.

Finally, my family and friends have always been there for me. I couldn't have completed this work without their help.

Abstract

As the public demand for electric vehicles and consumer electronics grows at an exponential rate, traditional energy storage systems like lithium-ion batteries are proving to be insufficient. A potential candidate to replace these conventional systems is the **lithium metal battery**. However, replacing the anode of lithium-ion batteries with lithium (Li) metal comes with its own challenges. Safety concerns and capacity loss during cycling (discharge-charge) are caused by internal dendrite formation and infinite volume change of the Li metal. In this work, two different strategies have been explored to counter these issues:

1. 3 dimensional metallic host for Li metal
2. Surface layer deposition

As a 3D metal host, **a 3D porous nickel (3DPNi) substrate** was used. It was fabricated in-house through a facile template-free electrodeposition process. Detailed electrochemical Li cycling tests were performed using a symmetric cell to investigate the performance of the substrate. Different aspects of the Li cycling like substrate structure and morphology, electrolyte modification (with $LiNO_3$), kinetics of Li^+ diffusion and the electrochemical impedance performance of the substrate were investigated. The 3DPNi substrate was also tested for its compatibility with sodium metal. To investigate the effect of surface layer deposits, **atomic layer depositions (ALD)** of Al_2O_3 and TiO_2 were done on planar nickel substrates. Each of these were subjected to electrochemical Li cycling tests.

Our results show that the 3DPNi substrate can be effectively cycled with Li for up to 300 cycles at a capacity of 0.5 $mAh \cdot cm^{-2}$ and a current rate of 1 $mA \cdot cm^{-2}$. Increasing the capacity to 3 $mAh \cdot cm^{-2}$ (6 times) at the same current rate resulted in up to 60 cycles. It was also found out that this substrate could be used for sodium metal cycling. ALD on planar substrates have enabled the Li metal to be cycled for more than 300 cycles without failure, albeit at a capacity of 0.25 $mAh \cdot cm^{-2}$ and a current rate of 0.125 $mA \cdot cm^{-2}$. Hence, our study confirms that both the methods significantly improve the performance of the lithium (and sodium) metal battery.

Keywords: *Lithium metal battery, sodium metal battery, 3D porous nickel, atomic layer deposition, dendrite formation*

Contents

List of Figures

1

Introduction

1.1. Current research scenario & Motivation

The need for energy storage systems can be juxtaposed with the advances in technology. Humans have developed sophisticated technological devices from extraterrestrial space rovers to quantum computers and we need energy to power them. This has in turn, motivated them to improve our energy storage systems. Maximum focus has been given to the sphere of electrochemical energy storage, since it is one of the most economical and portable forms of energy storage. A battery is one of the most ubiquitous form of electrochemical energy storage.

Tracing the evolution of batteries from the voltaic pile to the Lithium-air battery, it is evident that the research has been focused on improving three aspects[1]:

1. Energy density - The total amount of energy (charge) that can be provided by the cell. It is expressed as either gravimetric energy density ($Wh \cdot kg^{-1}$) or volumetric energy density ($Wh \cdot l^{-1}$). Areal capacity with the units $Wh \cdot cm^{-2}$ may also be used.
2. Power density - The amount of energy (charge) released per unit time. It has the units $W \cdot kg^{-1}$ or $W \cdot l^{-1}$.
3. Cycle life - The number of charge and discharge cycles that a battery can achieve before its capacity is exhausted.
4. Safety - Lithium (Li) & sodium (Na) metals are extremely active due to their low electrochemical potential(vs. standard hydrogen electrode). This gives rise to safety concerns and it must be made safe in order to be commercialized.

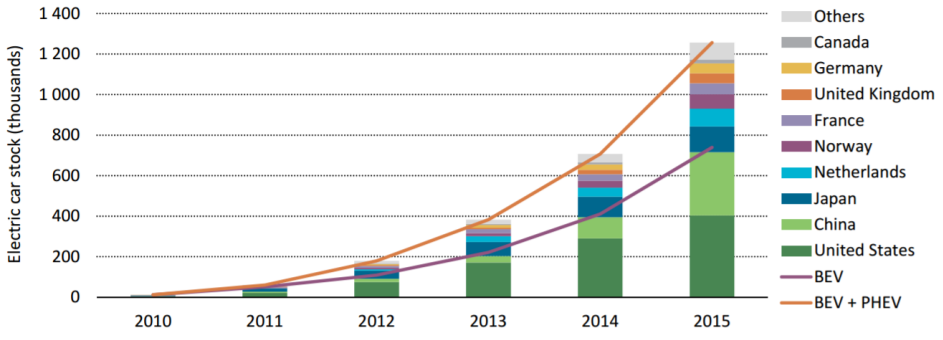

Note: the EV stock shown here is primarily estimated on the basis of cumulative sales since 2005.

Sources: IEA analysis based on EVI country submissions, complemented by EAFO (2016), IHS Polk (2014), MarkLines (2016), ACEA (2016a), EEA (2015) and IA-HEV (2015).

Figure 1.1: Global plugged-in electric vehicle sales. [2]

The major portion of the current thrust for battery research is provided by the need to commercialize electric vehicles. Figure 1.1 shows that the increase in global demand for battery electric vehicles

(BEVs) and plug-in hybrid electric vehicles (PHEVs) have been rising steadily from the beginning of this decade. The year 2015 saw the global threshold of 1 million electric cars (including battery electric, plug-in hybrid electric, and fuel-cell electric vehicles) on the road exceeded, reaching up to 1.26 million. This has been possible due to the decreasing costs and increasing efficiency of the batteries. Battery costs have gone down by a factor of 4 since 2008[2].

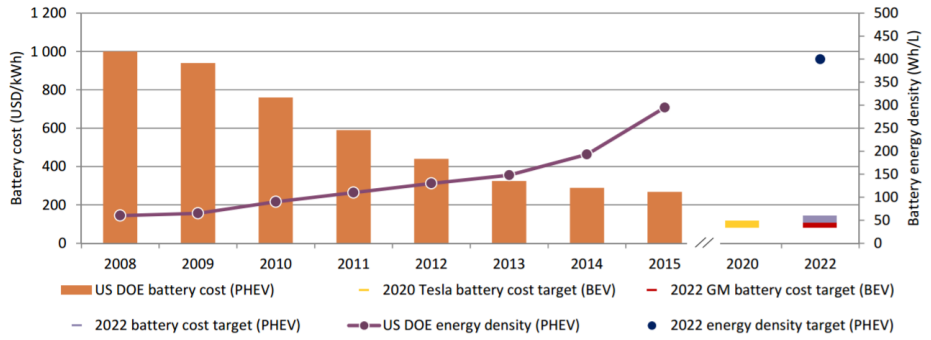

Notes: USD/kWh = United States dollars per kilowatt-hour; Wh/L = watt-hours per litre. PHEV battery cost and energy density data shown here are based on an observed industry-wide trend, include useful energy only, refer to battery packs and suppose an annual battery production of 100 000 units for each manufacturer.

Sources: US DOE (2015 and 2016) for PHEV battery cost and energy density estimates; EV Obsession (2015); and HybridCARS (2015).

Figure 1.2: Cost of battery systems and its energy density from 2008. [2]

However, for EVs to achieve cost parity with conventional internal combustion engines (ICEs) significant progress in terms of battery performance and economic feasibility is necessary.To this end, metal batteries which employ metals (Li, Na etc.) as the anode offers a significant upgrade over the existing Li-ion batteries. Lithium metal boasts of the highest theoretical capacity (3860 $mAh{\cdot}g^{-1}$, or 2061 $mAh{\cdot}cm^{-3}$) and lowest electrochemical potential (–3.04 V vs. SHE) for any element[3]. Similarly, sodium has a relatively high theoretical capacity of 1166 $mAh{\cdot}g^{-1}$[4]. With the goal of increasing the capacity of battery systems, a lot of the current research is focused on systems like Li-Air, Li-S and their Na counterparts. However, when considering the cycle life and safety aspects of such batteries it is not close to commercialization.

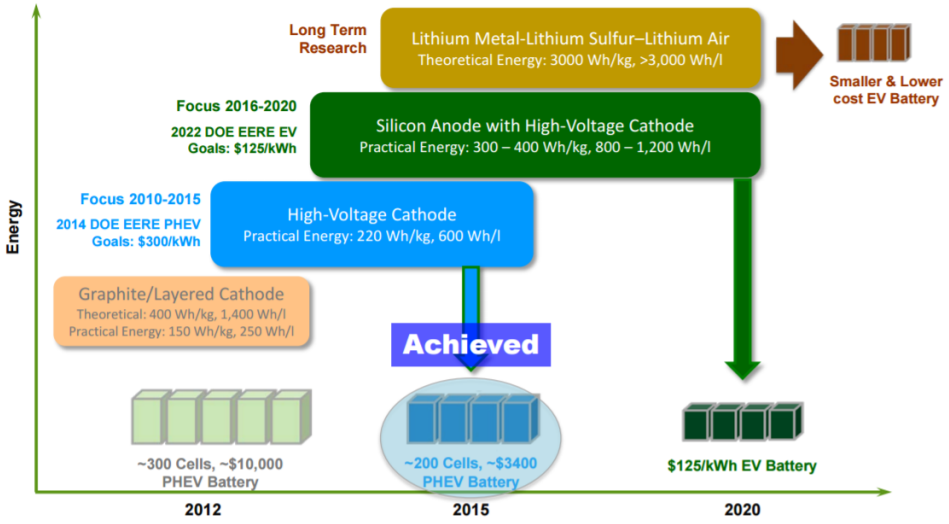

Figure 1.3: Evolution of Li based battery system research. [5]

1.2. Scientific background

This section provides the reader with the necessary scientific information to understand and appreciate the work done in the project. Relevant scientific publications are referenced when needed, to direct the reader towards extensive reading material.

1.2.1. Battery Basics

A battery may be defined as a system that generates electrical energy by the direct conversion of chemical energy stored in an electrode material through an electrochemical reaction. In order to understand the basic working and chemistry of batteries, it is important to know the basic structure of a battery. A cell is the fundamental unit of a battery. Many cells combine together to form a battery. However, over the years batteries have also come to represent a single cell.

In the simplest of terms, an electrochemical cell consists of two conducting electrodes, separated by an electrolyte and an external load (or any electron conducting medium). During the discharge of the cell, each electrode performs a specific function. The electrode which supplies the electrons and the positive ions is called the anode (negative terminal) and the other electrode which accepts the two charged species is called the cathode (positive terminal). In other words, oxidation takes place at the anode whereas reduction takes place at the cathode. The electrolyte, which separates the two electrodes, offers a path for the conduction of the positive ions while remaining electronically insulating. A separator is also used to prevent direct physical contact between the two electrodes. The electrodes are connected to the external circuit through metallic plates called the current collectors. The two charged species (positive ions and electrons) produced at the anode, travels through their respective conduction path and gets reduced at the cathode. Thus, the electrical circuit is completed and we can extract the electrical energy through the external load. During charging, the charges are forced to flow in the opposite direction, from the cathode to the anode.

In the cell, the two electrodes (anode and cathode) are of different electric potential. This creates a potential difference when immersed in the electrolyte and connected through an external load. This potential difference is also known as electromotive force (V). The electric potential maybe defined as the potential energy of a unit charge within an electric field and this drives the current in the electric circuit. This potential difference leads to redox reactions at each electrode, which generates electrons which pass through the external circuit. The redox reactions at the electrode continue until the equilibrium is reached.

Batteries that can only be used once are called primary batteries. These batteries can only be discharged once. Secondary batteries are those that can be charged (or brought back to its original state) by passing electricity in the direction opposite to that of the discharge current. Thus, these batteries can be used multiple times.

1.2.2. Thermodynamics

The electrochemical reaction which occurs during the discharging of a battery is responsible for the electric energy that the battery can deliver. Hence, the chemical work is directly linked to the electrical work. Consider the following electrochemical reaction at a given electrode:

$$wA + xB \rightleftharpoons yC + zD \tag{1.1}$$

where, w, x, y and z are stoichiometric coefficients of A, B, C and D, which are different chemical species. From standard thermodynamic principles, the Gibbs free energy for the above reaction is given as,

$$\Delta G = G^o + RT \ln(a_C^y a_D^z / a_A^w a_B^x) \tag{1.2}$$

where, a is the activity of the species. At equilibrium, the electric work (W^{rev}) is the maximum possible electric energy that can be extracted (W^{max}). When the battery is undergoing a chemical reaction during the discharge, this can be correlated to ΔG, the change in Gibbs free energy.

$$W_{rev} = W_{max} \tag{1.3}$$

$$-W_{max} = \Delta G \tag{1.4}$$

As we know, electric energy is associated with the flow of charge Q under an electric potential E. Therefore,

$$W_{max} = QE \tag{1.5}$$

Here, Q may be represented as a product of the number of electrons in the cell and the elementary charge. The number of electrons, n_e, is the number of moles multiplied by the Avogadro constant (N_A = 6.023 $\times 10^{23}$). Therefore,

$$Q = n_e e \tag{1.6}$$

$$Q = nN_A e \tag{1.7}$$

$N_A e$ is equivalent to the Faraday constant (F). It is defined as the amount of electric charge per mole of electrons. The value of the constant is 96485 C/mol. So,

$$Q = nF \tag{1.8}$$

Substituting this is in equation 1.5, we get,

$$W_{max} = nFE \tag{1.9}$$

This represents the electrical energy generated by the flow of 'n' moles of electrons due to the potential difference between the two electrodes. From equation 1.4, we know that this potential energy (electromotive force of the cell) is a result of the change in Gibbs free energy (ΔG) during equilibrium. This gives us the relation,

$$\Delta G = -nFE \tag{1.10}$$

When the reactants and products are in a standard rate, the electric potential is denoted by E^o. This modifies the previous equation for the standard condition as,

$$\Delta G^o = -nFE^o \tag{1.11}$$

The equations 1.2 and 1.11 can be used correlated with the concentration of components involved in the electrochemical reaction using the Nernst equation as,

$$\Delta G = \Delta G^o - RT \ln(a_C^y a_D^z / a_A^w a_B^x) \tag{1.12}$$

1.2.3. Li-ion batteries: A materials perspective

This section has been prepared from [1] and the reader is referred to the same source for an extended reading.

Anode

It is interesting that lithium metal was the first anode material of choice for lithium secondary batteries. However, due to the safety issues mentioned in the previous section, it was soon replaced by a safer alternative. Carbon-based anode materials like graphite was responsible for the commercialization for lithium secondary batteries in 1991. To its credit, lithium ions could be inserted into these materials which helped it to maintain a stable state. Also, there was no appreciable change in the crystal structure of the carbon-based materials during this intercalation and deintercalation process. Another class of anodes work on the basis of alloying and dealloying with Li. While being charged, these materials react with Li in a specific voltage range to become alloys. Upon discharging, the Li de-alloys and they return to their original state. Some examples are silicon, tin, indium and lead.

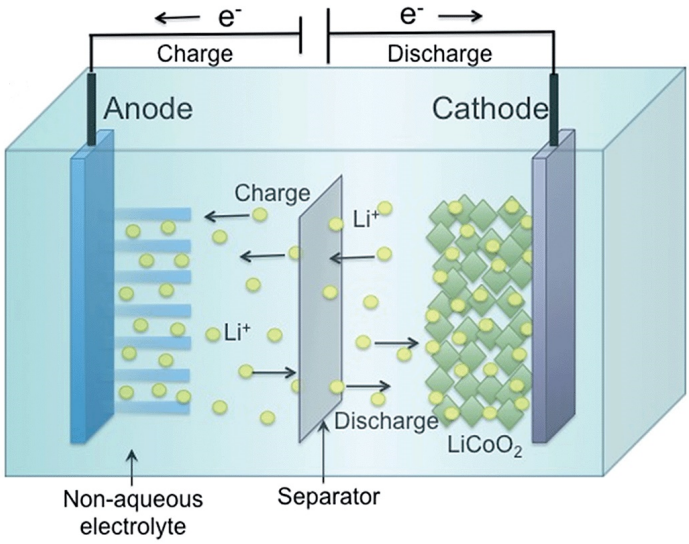

Figure 1.4: Schematic representation of a Li-ion battery. [6]

Cathode

$LiCoO_2$ was the cathode material when Li secondary batteries were commercialized in 1991. Other important materials include spinel $LiMn_2O_4$ and $LiNiO_2$. Further research has helped to combine the advantages of the three materials in the three-component Li[Ni, Mn, Co]O_2 systems. $LiFePO_4$ (olivine) is also actively studied. As is evident, transition metal oxides with intercalated Li is a popular choice for cathode materials. However, in the search for batteries with higher energy density, researchers are moving towards other cathodes like anionic redox materials[7], Li-O_2[8] cells and Li-S (sulphur) cells[9].

Electrolytes

As mentioned earlier, an electrolyte is an electronically insulating medium which facilitates the motion of ions through the cell. There are different kinds of electrolytes. Some of the major types are liquid electrolytes, solid electrolytes and polymer electrolytes. Liquid electrolytes generally consists of a solvent and salts (for example like $LiPF_6$). Solid electrolytes are based on inorganic compounds or polymers. The polymer electrolytes are composed of a polymer and salts. All types of electrodes are expected to have high chemical stability towards the other materials used in the battery. It must also be electrochemically stable in the potential range of the redox reactions happening at the two electrodes. Apart from this, it must be also suitable for use in a wide temperature range.

Separators

The separator is a thin porous membrane that prevents the physical contact between the two electrodes inside the cell. This is generally employed in liquid electrolyte based cells where there is no physical barrier between the electrodes. Thus, it plays the crucial role of ensuring that the cell does not short-circuit upon assembly. It also has to facilitate efficient flux of ions between the electrodes. The separator should be electrochemically stable in the voltage window of the cell and must be sufficiently wetted by the electrolyte. A typical separator used in batteries are single layer or multilayer polymer sheets made of polyolefins[10].

Current collectors

A current collector serves as a pathway for current from the electrodes to the external circuit. Typically, electrode material is applied onto the current collectors together with binders, conductivity additives, and other processing additives. Metals are usually employed as current collectors. In a normal Li-ion battery, copper is used at the anode side whereas aluminium is used at the cathode side[11].

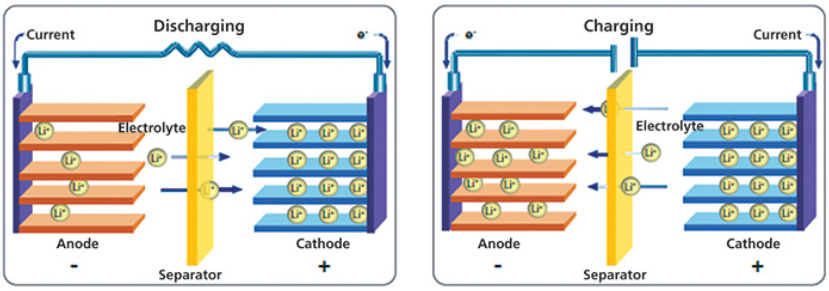

Figure 1.5: Movement of Li^+ ions, electrons and electric current during the discharge and charge cycles. [12]

1.2.4. Lithium metal batteries

In Li metal batteries (LMB), the negative electrode (anode) is Li metal as compared to graphite or silicon in the Li-ion batteries. The rest of the battery architecture remains the same in principle. Some examples of LMB are Li-LMO (lithium transition metal oxides), Li-S and Li-air systems. It is clear from figure 1.6 that Li metal-based batteries offer a definite pathway to increase the specific energy of battery systems. Its development would be crucial for the EV market to sustain its growth and compete with existing fossil fuel-based systems.

Why do we need Li metal batteries?

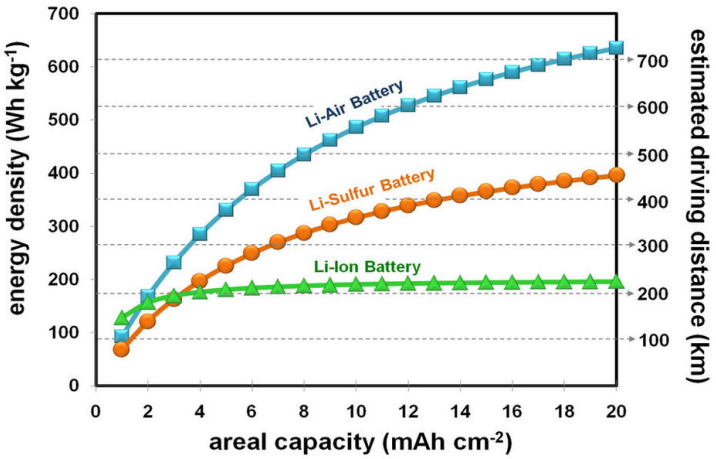

Figure 1.6: Relation between the energy density, areal capacity and the estimated driving distance of an electric vehicle of different battery cells. [13]

The conventional LIBs which uses the graphite anode and $LiCoO_2$ cathode is proving insufficient to the meet the requirements of the current consumer electronic devices and electric vehicles market[14]. And unfortunately, the room for improvement of the battery performance is limited due to the low theoretical specific capacities of the materials used in LIBs[15][16]. A Li metal-based battery is a significant upgrade in this direction. New battery systems like Li-S and Li-air offer higher theoretical energy which could translate into successful commercialization at a later stage.

However, the commercialization could take a few decades. Fortunately, attaining an energy density of 1700 Wh/kg is an achievable target since it amounts to only about 14.5% of the theoretical energy content of the system[17]. For comparison, current state-of-the-art Li-ion cells can reach a specific energy of 250 $Wh{\cdot}kg^{-1}$, which is still an order of magnitude lower than the practical value of petrol (gasoline). A Li–LMO cell can deliver a specific energy of 440 $Wh{\cdot}kg^{-1}$. Moving to Li–S and Li–air systems can boost the specific energy to 650 $Wh{\cdot}kg^{-1}$ and 950 $Wh{\cdot}kg^{-1}$, respectively[3].

Li metal anodes

The cornerstone for Li metal-based battery systems like Li-air and Li-S is the Li metal anode. As mentioned before, Li metal is the ideal anode material in theory because of the following reasons[1]:

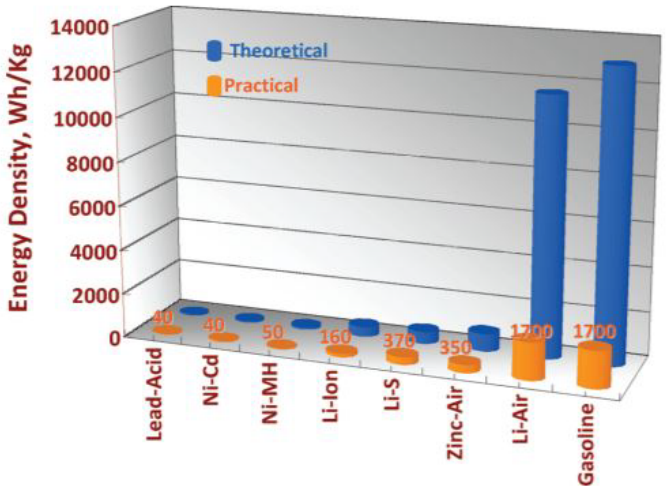

Figure 1.7: Comparison of the energy density of various battery systems with gasoline. [17]

1. Electropositivity: Highest among elements (-3.04 V vs. Standard Hydrogen Electrode)
2. Weight: Lightest metal (Standard atomic weight of 6.941 $g \cdot mol^{-1}$ & specific gravity of 0.53 $g \cdot cm^{-3}$)
3. Highest specific capacity : 3860 $Ah \cdot kg^{-1}$
4. Atomic radius: Smallest among metals which facilitates better diffusion (0.76 Å).

Unfortunately, these factors can lead to disadvantages as well. Lifetime, efficiency and safety are the three most important concerns of Li-metal batteries as of now. It is imperative that the factors causing these issues should be studied and understood from a fundamental level before we can look towards practical solutions to overcome them. The root cause of the problems faced by Li metal anodes is the **heterogeneous nature of Li cycling** in a cell, i.e deposition and stripping of Li ions (Li^+) onto and from the Li metal during the charging and discharging process[3]. However, there are many facets about this process that needs to be examined carefully.

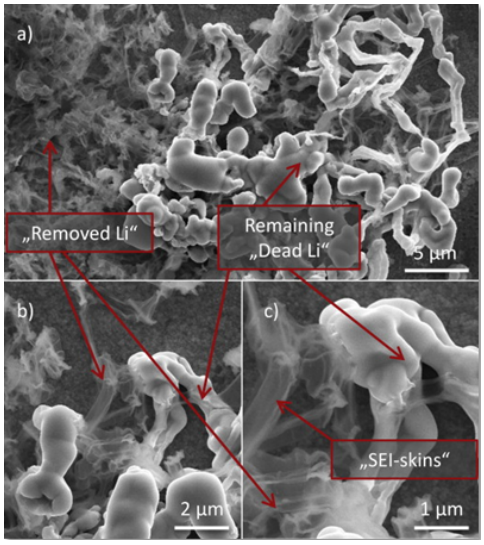

Figure 1.8: Li dendrites on Cu electrode as seen after OsO_4 exposure. [18]

Solid electrolyte interphase - As we have seen before, Li metal boasts of the highest electropositivity among all the elements. This enables it to donate electrons to form positive ions very easily. Hence, virtually any electrolyte can be reduced at the Li surface. LMBs generally use Li salts

like Bis(trifluoromethylsulfonyl)amine lithium salt (LiTFSI) or Lithium hexafluorophosphate ($LiPF_6$) dissolved in organic solvents like ethylene carbonate (EC), propylene carbonate (PC), dimethyl carbonate (DMC), ethers (e.g. 1,2-dimethoxyethane (DME) etc. The reduction potential of such organic solvents is usually below 1 V (vs. Li^+/Li). Thus, exposure of the electrolyte solution (Li salt + organic solvent) to bare Li combined with the application of current, leads to spontaneous reactions (milliseconds or less) between Li and the electrolyte species. These insoluble reaction products formed due to the reaction between Li^+, anions, and solvents are deposited on the metallic anode surface forming a layer with thickness in nanometer scale - this layer is called SEI or the solid electrolyte interphase[19]. The SEI layer forms a passivation layer on the Li metal which enables the cell to be operated under reducing environment and provides a voltage window up to 4 V and above. From a chemical perspective, this layer is electronically insulating while being conductive towards Li^+. However, to ensure the efficient cycling of the cell, the SEI formed must be homogeneous in composition, morphology and ionic conduction. Local variations in any of these factors can directly lead to the failure of the cell[3].

Dendrite formation - Li metal, like most other metals, deposits in dendritic (branched tree-like) form[20]. This characteristic growth of dendrites during cycling is responsible for three major issues that are detrimental to the efficient working of LMBs. They are:

1. Safety - The growth of dendrites from the Li metal anode can penetrate the SEI layer and the separator and lead to the formation of an internal physical contact between the two electrodes in a cell. This leads to thermal runaway and explosion hazards, caused due to the internal short-circuiting of the cells[3].
2. Volume change - The general process of Li deposition and stripping involves an infinite volume change. This contributes to the weakening the SEI layer due to mechanical stress which leads to its fracture. This process facilitates Li dendrite growth which further aggravates the problem[16].
3. Capacity fade - The heterogeneous nature of Li cycling as well as the dendrite formation leads to cracks in the SEI layer. This causes new SEI to be formed in these regions. This coupled with the breaking away of Li dendrites which cannot take part in the cycling process, leads to ”dead lithium”. This results in the loss of capacity of the system[3].

Mechanism of dendrite growth

The mechanism of dendrite growth and its propagation has been extensively studied[21][22]. However, there is no one theory that satisfactorily explains the whole process. In this report, we shall look at two theories which can rationalize this phenomenon, albeit with some limitations.

Dendrites maybe divided into three kinds based on their morphology - needle, fractal and mossy. This can indeed lead to confusion while interpreting the phenomenon[23]. Mossy dendrite structures are unique to electrodeposition and it depends on the components and design of the cell[24]. The spontaneous formation of SEI plays an important role in the evolution of the dendrites. Depending on the structural and morphological heterogeneity on the Li metal surface, the SEI layer formed will be prone to variations in thickness and ionic conductivity. This leads to difference in impedance for ion flow along the layer, of which some regions would have low ion impedance. Even though the origins of these ”hot spots” remain unclear, it can be safely assumed that Li^+ ions will choose these paths of least impedance during the deposition process. This leads to preferential Li^+ ion deposition (plating) in these spots. As can be expected, this leads to a localized volume expansion which cannot be accommodated by the SEI. The SEI layer in that region breaks as a result, leading to exposure of fresh Li which opens up pathways for further Li^+ ion deposition. This causes the three dimensional growth of mossy dendrite structures. Also, freshly deposited Li sites have lower impedance than other sites along the SEI layer due to its reduced thickness. This further propagates the preferential growth of dendrites in the same location. During the stripping process, Li is preferentially removed from these dendrite structures. Stripping happens from the previously mentioned ”hot spots” or low impedance sites. This creates a reduction in volume which causes the SEI layer to fracture again. The stripping process also forms isolated Li (known as ”dead Li”) which cannot take part in the electrochemical cycling anymore, leading to loss in cell capacity[23]. The formation of new SEI after every fracture also leads to loss of capacity due to irreversible consumption of Li^+ ions. Hence, a mechanically robust, flexible or elastic SEI layer is essential to the success of Li metal anode.

Kinetic model of dendrite growth - Sand’s time

Although several kinetic models have been proposed to the describe the Li dendrite formation, the most widely accepted one is based on Sand’s time[25]. The occurrence of Li ions near the Li metal

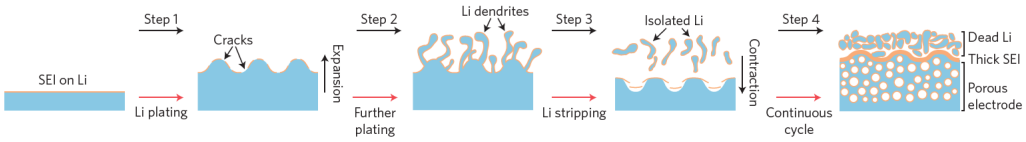

Figure 1.9: Schematic representation of the Li plating and stripping process. The repetition of steps 1-3 during cycling leads to the ultimate failure of the battery. [3]

anode results from the charge at a high current density, as well as the consumption of Li salt anions in the Sand's time. This results in the lack of Li^+ layer, which when coupled with the local space charge layer, may be regarded as the main reason for the formation of Li dendrite. The "Sand's time" τ is dependent on the parameters of Li^+ ions and electrons empirically as follows,

$$\tau = \pi D \frac{eC_o(\mu_a + \mu_{Li^+})^2}{2J\mu_a} \tag{1.13}$$

where τ is the initial time of Li dendrites growth, C_0 is the initial concentration of Li salt, D is the diffusion coefficient, e is the electronic charge, and J is the effective electrode current density. μ_a and μ_{Li^+} formula are the mobility of anions and Li^+ ion, respectively. This equation tells us the parameters that can be modified to delay the growth of Li and in turn realise the goal of dendrite-free Li metal anodes. [26]

Fortunately, a lot of research on Li metal anode batteries has been published in the recent years. Na metal anode batteries are slowly gaining traction because they offer a cost-effective alternative to Li-based systems, especially where total weight and energy density are of minor importance like grid energy storage for renewable energy sources[27]. However, compared to Na, a lot of study has been done on the fundamental aspects of Li metal anodes. To summarize, the major drawback of LMB is the heterogeneous behaviour of Li plating and stripping. This is in turn is responsible for dendrite formation which eventually leads to short circuit and capacity fade of the battery.

In order to tackle these issues with safety and capacity degradation of Li metal anodes, researchers around the world have tried different approaches. They can be broadly classified into the following[3]:

1. Electrolyte modifications - Various additives have been incorporated to the electrolyte to improve the efficiency. These additives are capable of modifying the metal-electrolyte interphase (SEI) to ensure a more homogeneous plating-stripping behaviour. A few examples are flourinated compounds like HF[28], $LiNO_3$ and Li polysulphide[29] and using caesium or rubidium ion additives as a self-healing electrostatic shielding mechanism[30]. Also, advanced solid electrolytes can pose as a physical barrier for the propagation and growth of dendrites. Inorganic ceramic electrolytes and solid polymer electrolytes are the two main types of such electrolytes. The inorganic ceramic electrolytes include Li-ion conductive species like sulphides[31], oxides[32], nitrides[33] and phosphates[34]. Solid polymer electrolytes are those which blend Li salts with polymers[35].

2. Interface engineering - Researchers have tried to modify the interface between the Li metal and the electrolyte (SEI) to ensure a favourable plating-stripping behaviour. The main objective behind this approach is to stabilize the SEI formed. Some techniques involved are creation of an artificial protective layer on the anode before the cycling[36][37], nanostructuring chemically stable and mechanically strong scaffolds to strengthen the SEI formed during cycling[38][39] and homogenizing Li-ion flux by increasing the surface area of the anode current collector[40][41].

3. 3D stable hosts - Since Li plating & stripping leads to infinite volume change, efforts have been made to contain Li within stable host materials like layered graphene oxide[42] or a polymeric matrix[43].

4. Guided Li plating & protection - A seeded growth control mechanism where the Li nucleation and growth were controlled on specific sites was another method used to tackle heterogeneous Li deposition during cycling[44].

As can be seen from the above references, dendrite-free metal anode batteries has gained significant attention over the past few years. Despite all the efforts, commercialization of this technology is still not feasible due to economic as well as safety reasons.

1.2.5. 3-dimensional Porous Nickel

The 3DPNi substrate forms a central part of this project. It is necessary to understand its fabrication and structure-morphology characteristics to understand its role in the suppression of dendrites.

Fabrication - Hydrogen Bubble Dynamic Template Method

The 3DPNi substrate is prepared using the hydrogen bubble dynamic template (HBDT) method. This method offers a template-free, simple, fast, one-step method to electrochemically fabricate materials with high surface area, high porosity and controlled morphology. These materials may be used in catalysis, sensing, energy among other fields[45].

The HBDT method is a variation of the standard galvanostatic electrodeposition from an aqueous solution. Similar to the typical electrodeposition process, this method involves deposition of the metal on the working electrode through the reduction of the solvated species. However, the HBDT method differs from the standard electrodeposition process in that it involves the application of relatively high cathodic overpotential. This results in the H^+ ion in the aqueous electrolyte being reduced to H_2 gas and it bubbles off the working electrode (and the growing metal deposit), disrupting the metal deposition process. The different reactions occurring may be summarized as follows:

1. $2H^+(aq) + 2e^- \rightarrow H_2$
2. $H^+(aq) + e^- \rightarrow H(adsorbed)$
3. $H^+(aq) + H(adsorbed) + e^- \rightarrow H_2$
4. $2H(ads) \rightarrow H_2$
5. $M^{n+}(aq) + ne^- \rightarrow M(s)$

The bubbles acts as a dynamic template during the process and the metal deposition happens through free space between the bubbles. Hence, we eventually get a structure with macro and nano-sized pores. The generation and dynamics of the bubble formation as well as the overpotential significantly affect the nature of deposition and hence, offers us ways to modify the structure and morphology of the deposit. Thus, the Hydrogen Bubble Dynamic Template (HBDT) technique enables us to create porous foam structure in a clean and efficient manner.

Preliminary work in this field was done by *Marozzi et al.* in early 2000s[46][47]. Apart from the obvious advantages of being simple, clean and fast, this technique also offered the possibility of varying electrodeposition parameters to obtain diverse structures. To this end, the electrolyte bath composition, the current density of deposition (cathodic overpotential) and the duration of deposition were the parameters varied in this work:

1. Electrolyte bath composition - Varying the amount of surfactant in the bath offers a way to alter the morphology of the deposit by controlling the dynamics of bubble formation. The surfactant used in the work is Polyethylene glycol or PEG. It is a surfactant that significantly affects the bubble behaviour, as it hinders the coalescence of bubbles by reducing the surface tension at the bubble-liquid interface[45]. It also results in smaller pore sizes in the final deposit structure. PEG is also used as a common additive in acidic copper electrodeposition, to increase the overpotential and impede the copper deposition to obtain 'bright' coatings. This essentially means that it makes it harder for the copper deposit to have dendritic nature and smoothens the surface. Under the same principle, the same effect is hoped to be seen nickel deposits[48].

2. The current density of distribution - The current applied has a marked effect on the generation and kinetics of bubble formation. The bubble density increases with the current density. At higher current rates, larger amount of H^+ ions from the electrolyte are reduced to H^2 gas. Therefore higher amount of bubbles are formed. The instability of larger bubbles at higher growth rates decreases the residence time of the bubbles at the working electrode. This increases the overall porosity of the deposit but the vigorous stirring action of the bubbles reduces the mechanical integrity of the 3D structure. [45].

3. The duration of deposition - The time of deposition decides the thickness of the deposit formed. As the duration of current applied increases, a thicker deposit is obtained.

The fundamentals of bubble generation and the dynamics of its growth need to be understood further to improve our control on morphology and the structure of the final deposit. There are different parameters that maybe varied to obtain different deposits. This method may be extended to many other different metals - to create both monometallic or bimetallic deposits.

1.2.6. Sodium metal batteries

Due to the concerns about the sustainability of global lithium resources, researchers have been looking towards sodium metal batteries as alternative energy storage device.

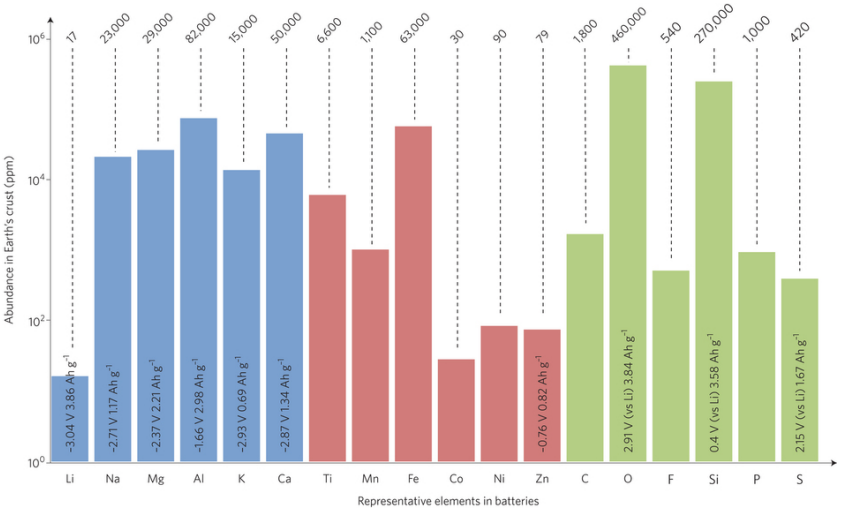

Figure 1.10: The abundance of the different chemical elements currently used in battery systems (values in ppm is given on top). The standard redox potentials of metal anodes together with their capacities are given in the rectangles). [49]

From the figure 1.10, it can be seen that Na metal boasts of high natural abundance. Also, it has a low cost of production which enables it to be used for mass commercialization. Based on some estimates, the raw materials for Na metal batteries are estimated to be 30 times cheaper than its Li counterparts.[27] Even though Na metal is heavier than Li, Na-based batteries find use in scenarios which require stationary energy storage systems like grid storage. The Na metal anode, which could be used in Na-S and Na-air battery systems, has high theoretical capacity of 1166 $mAh{\cdot}g^{-1}$ and low redox potential of -2.7 V (vs. SHE). However, like Li metal anodes, Na metal anodes also suffer from the safety and capacity fade problems due to the inherent dendrite growth mechanism, which is severe than Li in some cases. Na metal anodes also lead to decomposition of electrolytes due to sodium's high reactivity, which is higher than that of the Li metal[50].

1.2.7. Research Methodology

The motivation for this graduate thesis work was to contribute towards the goal of realizing a stable, safe and efficient Li (and Na) metal anode.The idea of using a 3DPNi substrate to tackle Li dendrite growth is inspired from the various approaches to create dendrite-free Li metal batteries mentioned earlier.

The 3DPNi substrate is intended to be a current collector - like scaffold structure to contain Li metal on the anode side. The scientific rationale behind this approach is based on the following aspects:

- Sand's equation - 3DPNi is a conductive micro/nano-structured metallic network. This will distribute the electrode current density over a larger area which would reduce the 'J' term in the Sand's equation. This would increase the τ, or the initial time for dendrite growth. The distribution of current will also lead to homogenizing the Li^+ flux at the electrode. Hence, the start of the dendrite growth will be delayed.
- Volume change - The Li atoms will be deposited into the free volume of the 3DPNi structure. This foam structure will ensure that the Li^+ is deposited as small domains rather than a single block. This minimizes the overall Li volume change and also increases the active Li surface area. The stable 3D structure can also help to minimize the stress fluctuations within the cell.

The surface layer deposition helps in the formation of a artificial passivation layer. This passivation layer will homogenize the SEI layer formed and aid its stabilization. However, the mechanism of this process is still not understood clearly. It acts a physical obstacle for dendrite growth as well as stabilize the SEI layer formed on the electrode surface. Surface layers can also protect the electrode from corrosion due to the exposure to atmosphere and electrolytes. [51]. This will be discussed in detail in the 'Results' chapter.

1.3. Thesis structure

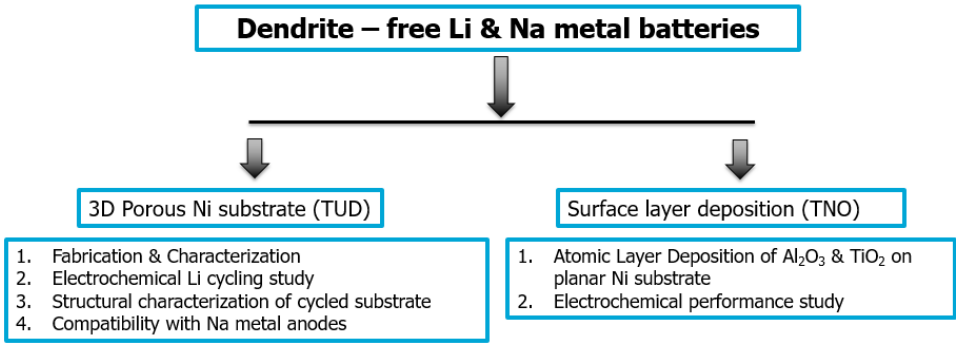

Figure 1.11: Thesis structure

The project involved the investigation of two different strategies to achieve dendrite-free Li metal batteries. One approach was to develop a **3-dimensional porous nickel (3DPNi)** substrate which would serve as a host and current collector for Li metal anode. The second approach was focused on studying the effect of different **surface layer depositions** on the Li metal cycling. The project can be divided into two stages:

1. 3DPNi substrate: In the first stage, the substrate was fabricated using galvanostatic electrodeposition. Following this, different kinds of substrates (with varying morphology and structure) were produced. They were then subjected to Li cycling in a symmetric cell to study the potential variation and Coulombic efficiency of Li cycling. A suitable substrate was chosen from studies by analyzing the performance of each of the substrate. This was followed by an extensive study of the Li cycling performance of the substrate under different conditions. In the next stage, the effect of modifying the electrolyte with $LiNO_3$ addition on the Li cycling performance was studied. The impedance to ion flux in the cell was also tested. Finally, the possibility of using the same 3DPNi substrate for Na metal batteries was explored.

2. Surface layer deposition: Two different depositions were carried out - titanium dioxide (TiO_2) and alumina (Al_2O_3). An electroplated planar Ni substrate was chosen as the substrate. The surface layers were deposited by atomic layer deposition (ALD) technique. The Li cycling performance of these substrates (with the deposition) was studied with a symmetric cell.

This report is divided into different chapters. The next chapter explains the experimental setup and procedures. This is followed by the results of the experiments and its discussion. The penultimate section explains the conclusions we have drawn from our work after which, future work that can be done as a continuation is suggested.

2

Experimental Procedures

The experimental section of this project can be divided into two:

- 3DPNi substrate - Fabrication, electrochemical Li cycling studies, structural characterizations and electrochemical Na cycling study
- Surface layer deposition - Fabrication and electrochemical Li cycling study

2.1. 3 Dimensional Porous Ni substrate

2.1.1. Fabrication

The Ni substrate was fabricated by galvanostatic electrodeposition using the hydrogen bubble dynamic template method. A simple two-electrode setup was used for the purpose. The working electrode was a polished Cu foil of 5cm^2, of which an area of 1 cm^2 was exposed to the electrolyte. The remaining part of the foil was insulated with scotch tape. The counter electrode was a Ni foil of larger area (10 cm^2). The electrodes were supported by sticking it to a glass plate and were kept at a fixed distance of 2 cm. The base electrolyte was prepared with 0.12 M $NiSO_4$.6/7-H_2O and 1.5 M NH_4Cl. All the chemicals were used as received. The electrolyte was prepared in the demineralised (demi) water. Both the electrodes were thoroughly washed with ethanol and demi-water before the electrodeposition. The bath was undisturbed during the deposition. The deposition was carried out in room temperature.

The surfactant concentration, current density of deposition and the duration of deposition were the parameters varied to produce different substrates and to study its effect on the electrodeposited nickel. Polyethylene glycol (molecular weight = 4000), referred to as PEG4000 from here on, was used as the surfactant.

Parameter	Variations
PEG Concentration (per 300ml H_2O)	100mg 150mg 200mg 500mg

Parameter	Variations
Current Density(A/cm^2)	3 5

Parameter	Variations
Deposition time(s)	30 60

Table 2.1: The parameters varied during electrodeposition

After the deposition, the Cu foil with the 3DPNi deposition was washed with demi-water thoroughly. Then, the Cu foil was removed from the glass plate and the insulating tapes were peeled off. Following this, the 3DPNi substrate of 1cm^2 was carefully cut from the remaining Cu foil. It was dried overnight (approx. 15 hours) at 60^oC in a vacuum oven, before transferring it into the argon glove box for the cell assembly.

2.1.2. Structural characterization

The structural characterization of the pristine 3DPNi substrate was done by X-ray Diffraction [Philps X'Pert MPD X-ray diffraction system)], Scanning Electron Microscopy and Energy Dispersive X-ray Spectroscopy (EDS) (SEM)[JEOL JSM - 6010LA].

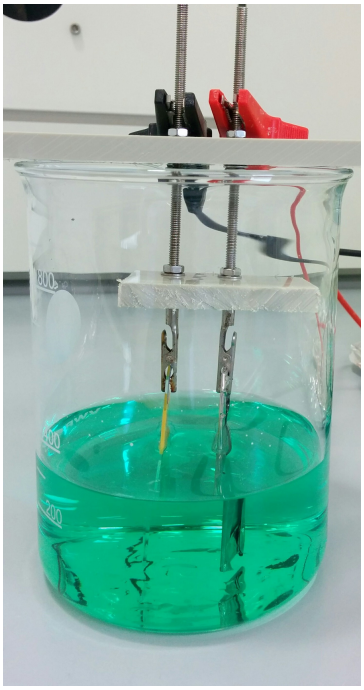

Figure 2.1: The electrodeposition setup.

2.1.3. Symmetric cell assembly

The electrochemical Li cycling tests were performed in a lab-designed symmetric cell. The parts of the cell include two stainless steel flanges, an O-ring (with a plastic support) in between the flanges, and a plastic vacuum clamp to hold them together. One of the steel flanges has a flat surface and the other one has a stainless steel plate attached to a steel spring to provide the necessary pressure and mechanical compaction inside the cell. The symmetric cells were assembled inside an Ar environment glovebox. The freshly fabricated 3DPNi substrate was used as the working electrode and the a Li metal foil (⌀ = 15 mm) was used as the counter electrode. A polymer separator (*Celgard*) was used to prevent contact between the two electrodes inside the cell. 1 M LiTFSI dissolved in DME (1,2 Dimethoxyethane) and DOL (1,3 Dioxolane) (1:1 in volume) was used as the electrolyte.

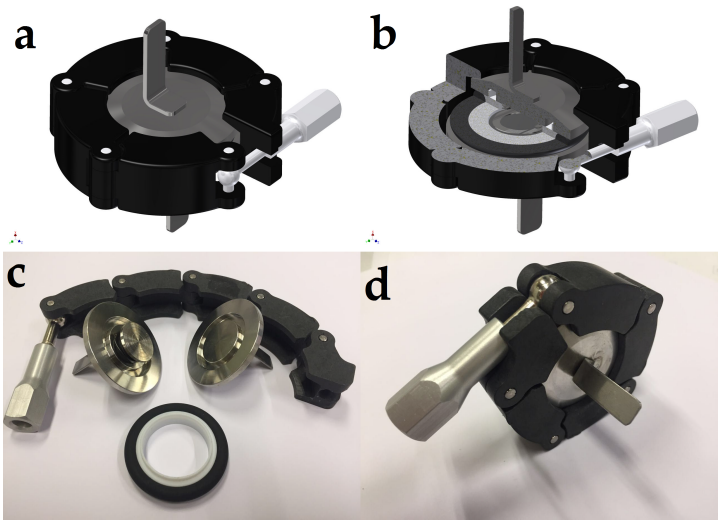

Figure 2.2: The symmetric cell used in this work: (a) - (b), design of the prototype cell; and photos of (c), all the cell components and (d) a closed cell. [52]

The cell was assembled through the following steps:

1. Cut the Li foil of 15 mm diameter and clean it thoroughly with a soft tissue soaked in DMC (Dimethyl carbonate). Let it dry.
2. Once it is dried, fix it to the steel plate attached to the spring. Removing the surface layer of the Li foil with a tweezer, aids in fixing the foil to the plate.
3. Carefully place the 3DPNi substrate onto the centre of the other flange (with the flat surface).
4. Put 4-5 drops of the electrolyte on the substrate and allow it to wet the entire area of the surface.
5. Place the separator on top of the substrate gently. Make sure the separator covers the entire substrate. Put 1-2 drops of the electrolyte on the surface to ensure that the separator is completely wet.
6. Carefully place the O-ring onto the steel flange with the substrate.
7. Close the cell by placing the other steel flange (with the Li foil) over it. Extra care is needed to ensure the substrate is not displaced from its position while the cell is closed.
8. Fasten the cell using the plastic vacuum clamp.

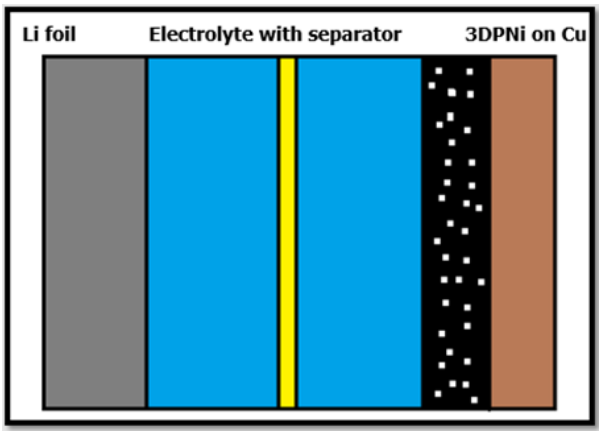

Figure 2.3: Schematic representation of the symmetric cell

2.1.4. Electrochemical Li cycling studies

Capacity & current rate

The capacity and current rate of the cell are two terms repeatedly used in this work. It is important to understand what they mean to follow the rest of the work.

1. Capacity - The amount of Li cycled in the cell. Since Li^+ ion species are involved in the cycling, the capacity of a cell is expressed in the units $mAh{\cdot}cm^{-2}$ - the unit of charge (per unit area). It stands for milli-ampere-hours per square centimetre.
2. Current rate - It refers to the rate at which the charged species (Li^+ ions) move inside the cell. The unit of this entity is $mA{\cdot}cm^{-2}$ - milli-ampere per square centimetre. The current rate multiplied by the time duration of discharge (in hours) gives the capacity of the cell.

For every cell cycled, we fix the capacity (amount of Li^+) and the current rate (rate of cycling Li^+). For example, a cell cycled with a capacity of 2 $mAh{\cdot}cm^{-2}$ at a rate of 0.5 $mA{\cdot}cm^{-2}$ takes 4 hours to completely discharge (plating on the 3DPNi substrate) the cell. The charging (stripping) time depends on the cut-off voltage. If the cut-off voltage is set at 0.5 V, the cell will be charged (or Li will be stripped from the substrate) until the voltage of the cell reaches 0.5 V.

Substrate tests

As explained in the previous chapter, the surfactant concentration, current density of deposition and duration of deposition alters the structure and morphology of the substrate. The different variations used are mentioned in table 2.1. Each of the different substrates produced were tested for its galvanostatic Li cycling performance in a symmetric cell. The potential and Coulombic efficiency of electrochemical Li cycling of the substrate were studied with the cell.

The electrochemical tests were done using a MACCOR - Series 4000 automated test system[53]. A test program with the following steps was written:

1. Rest for 2 hours to aid the voltage stabilization of the cell.
2. Initialize(clean) the substrate by cycling at 0–1 V (versus Li^+/Li) at 50 µA for five cycles to remove surface contamination and stabilize the interface.
3. Li cycling in the half-cell was done with a capacity of 0.5 $mAh \cdot cm^{-2}$ at a current-rate of 1 $mA \cdot cm^2$. The cut-off voltage for charging was 1V.

The first two steps mentioned (rest and cleaning) were performed as a standard for all the subsequent Li (and Na) cycling tests. The last cycling step mentioned above involves two parts - discharge and charge. During the discharge, 0.5 $mAh \cdot cm^{-2}$ of Li^+ was deposited from the reference Li foil (an infinite source) to the 3DPNi substrate. The deposition of this capacity was done at 1 $mA \cdot cm^{-2}$, which means that it was completed in 0.5 hours. In the charging step, the Li deposited on the substrate was stripped from it until the potential reached 1 V. The substrate which performed best in terms of the overpotential and Coulombic efficiency (explained in the next chapter) of the Li cycling process was chosen for further electrochemical studies.

Li cycling study - Capacity & Kinetics

Different electrochemical studies were performed to study the performance of the substrate and other metrics of the Li cycling process in detail. The various cycling tests done were as follows:

1. Study of the effect of the depositing different capacities ($mAh \cdot cm^{-2}$) of Li at the same current rate ($mA \cdot cm^{-2}$).
    - Constant current rate = 1 $mA \cdot cm^{-2}$
    - Varied capacities = 1, 2 & 3 $mAh \cdot cm^{-2}$
2. Study of the kinetics of Li cycling.

The cut-off voltage for charging in these tests was limited to 0.5 V. The kinetic aspects of Li deposition and stripping on the substrate was studied by reducing the stripping (charging) current rate at every 21st cycle. The substrate was subjected to Li cycling with capacity of 1 $mAh \cdot cm^{-2}$ at 1 $mA \cdot cm^{-2}$ for 20 cycles, after which for the next cycle (i.e at every 21st cycle) Li stripping was done at reduced current rate of 0.1 $mA \cdot cm^{-2}$. As a reference for comparison, a symmetric cell with a Cu foil (⌀ = 11.1125 mm) as working electrode was also prepared and cycled under the same corresponding conditions.

Electrolyte modification with $LiNO_3$

The normal electrolyte of 1 M LiTFSI in DME:DOL solvents (1:1 volume ratio) was modified by adding 1 wt% of $LiNO_3$. This addition of $LiNO_3$ to the electrolyte improves the Coulombic efficiency of the Li cycling process. This is due to formation of the passivation layer on the Li surface due to reduction of $LiNO_3$ which stabilizes the SEI [29] (explained further in the next chapter). To compare the performance of the new electrolyte with that of the normal one, a symmetric cell was prepared and cycled with capacity of 1 $mAh \cdot cm^{-2}$ at 1 $mA \cdot cm^{-2}$. The potential of the cycling and the Coulombic efficiency of the cell were studied.

Electrochemical Impedance Spectroscopy (EIS)

EIS is a widely used technique in electroanalysis to study the harmonic response of an electrochemical system. It tells us about the impedance characteristics of the cell. In EIS measurements, a minute sinusoidal variation is applied to the potential difference between the two electrodes in the cell (Li metal and the 3DPNi substrate in this case), and the resulting current is analyzed in that frequency domain in terms of impedance. The response of the system reveals the internal dynamics of the cell.

Impedance is a complex quantity that includes a real and an imaginary component. It arises in the case of alternating current (AC). It is analogous to resistance in the case of direct current (DC). The real component of the impedance corresponds to a resistance in-phase with the applied voltage. The imaginary component is a reactance 90^o out-of-phase with the applied voltage. The real and imaginary components of the impedance together give information about the kinetic and mass transport properties of the cell, and its capacitive properties. EIS results is either plotted using a Nyquist plot or a Bode plot. This work features the Nyquist plots in which the negative imaginary component of impedance (Y-axis) is plotted against the real component of impedance (X-axis).

EIS data for electrochemical cell systems can be modeled by equivalent circuit elements like resistor, inductor, capacitor etc. The electrochemical cell system used in this work, can be modeled using

the standard 'Mixed Kinetic and Diffusion Control' model. It represents a cell where the semi-infinite diffusion of the ionic species is the rate determining step, and a series solution resistance is the only other cell impedance[54][55].

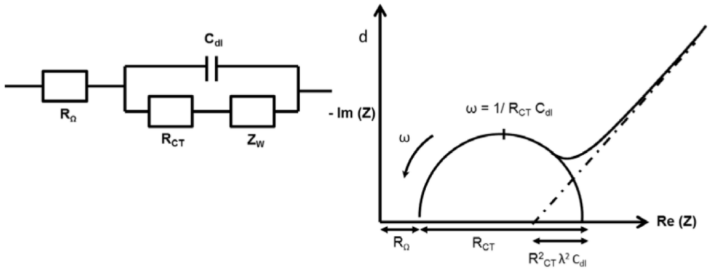

Figure 2.4: The equivalent circuit for mixed kinetic and charge-transfer control model (left) and the corresponding Nyquist plot. [56]

This model consists of a solution resistance (R_Ω), double layer capacitance (C_{dl}) and a charge transfer (R_{CT}) resistance. The double layer capacitance is in parallel with the charge transfer resistance and the Warburg element (Z_W) and this combination is in series with the ohmic resistance (solution resistance in this case). The corresponding Nyquist plot contains a semicircular arc intersecting the real axis (Z') at two places as shown in the figure above. The point of interception closer to the origin gives the value of solution resistance and the other intercept gives the total resistance (R_Ω + R_{CT}). The right part of plot is the low frequency domain and the left part represents the high frequency domain. The Warburg element is used to model the 'tail-like' region of the plot in the low frequency region. Th Warburg impedance denotes the diffusion of reactants toward or away from the electrode surface. The element models the Warburg resistance which is related to mass transfer resistance which has contributions from both the resistance and capacitance[56].

As with the structural studies, symmetric cells were prepared with the 3DPNi substrate was cycled in at a capacity of 1 mAh·cm^{-2} and a c-rate of 1 mA·cm^{-2} for specific number of cycles - 1, 2, 5, 20 and 50 cycles. Two kinds of cells were made - one with the normal LiTFSI in DME:DOL electrolyte and with $LiNO_3$ addition. A reference cell with a Cu foil (⌀ = 11.1125 mm) as working electrode was also prepared and cycled under the same conditions.

The EIS of the symmetric cell was done using Metrohm Autolab Potentiostat PGSTAT302N. The frequency range of the tests was 100 kHz to 0.1 Hz.

2.1.5. Structural characterization of cycled 3DPNi substrates

The structural analysis of the substrate after different stages of cycling were carried out by SEM study. The 3DPNi substrate was cycled in the symmetric cell at a capacity of 1 mAh·cm^{-2} and a c-rate of 1 mA·cm^{-2} for specific number of cycles - 1, 2, 5 and 50 cycles. Two kinds of cells were made, one with the normal LiTFSI in DME:DOL electrolyte and the other with $LiNO_3$ addition. After cycling, the cells were opened inside the glove box and the substrate was washed with Dimethyl carbonate (DMC) solvent and dried. It was then transported to SEM in an air-tight container.

2.2. Electrochemical Na cycling studies

To study the performance of the 3DPNi substrate with Na, a symmetric cell with the earlier configuration and Na metal as the counter electrode (⌀ = 15 mm) was prepared. The electrolyte used in this case was 1 M $NaPF_6$ (Sodium hexafluorophosphate) in DEGDME (Diethylene glycol dimethyl ether) solvent. Selected electrochemical cycling tests were performed with this symmetric cell to study the Coulombic efficiency and the potential of cycling.

2.3. Surface layer deposition on Ni substrate

Two different kinds of surface layer depositions were made on a planar Ni substrate of 13 mm diameter. They are:

1. TiO_2 layer of 'x' thickness by ALD.

2. Al_2O_3 layer of 'y' thickness by ALD.

The depositions were done at the TNO-Holst Centre, Eindhoven. For confidentiality reasons, the specific parameters of depositions cannot be shared. Symmetric cells of the same configuration mentioned before were made with the 1 M LiTFSI in DME:DOL (1:1 volume ratio) electrolyte. The cells were then cycled with a capacity of 0.25 $mAh \cdot cm^{-2}$ at a c-rate of 0.125 $mA \cdot cm^{-2}$. It is to be noted that the capacity and current rate used here is lower than the conventionally used values. This was in order to ensure that the the performance of the ALD coating would be the only parameter tested and that the cell would not fail due to other factors like high capacity or current rate. The cut-off voltage for charging was 1V. The Coulombic efficiency and the potential of Li cycling were studied.

2.4. Substrate handling

Both the 3DPNi and the ALD coated substrate should be handled carefully. The 3DPNi deposit on the Cu foil is extremely thin and hence can be easily scraped away. Therefore, it advised to handle the substrate through the bottom side, preferably using a spatula. Any physical contact on the deposit will result in the substrate being spoiled. Similar care is advised for the ALD samples as well, although the coating is much stronger in this case.

3

Results & Discussions

This chapter is divided into the following sections:

1. Fabrication & structural characterization of the pristine 3DPNi substrate
2. Electrochemical Li cycling performance
3. Electrochemical impedance spectroscopy (EIS)
4. Structural analysis of the of the cycled substrate
5. Electrochemical Na cycling performance
6. Surface layer deposition

3.1. Pristine 3DPNi - Fabrication & characterization

The 3DPNi substrate was fabricated through a galvanostatic electrodeposition. The surfactant (PEG4000) concentration in the electrolyte bath, current density and time duration of deposition were the parameters varied to develop different kinds of substrates. The Ni salt ($NiSO_4$.6/7-H_2O) is the source for the Ni ions. The addition of NH_4Cl improves the mechanical strength of the deposit and prevents formation of nickel hydroxide ($Ni(OH)_2$)[46].

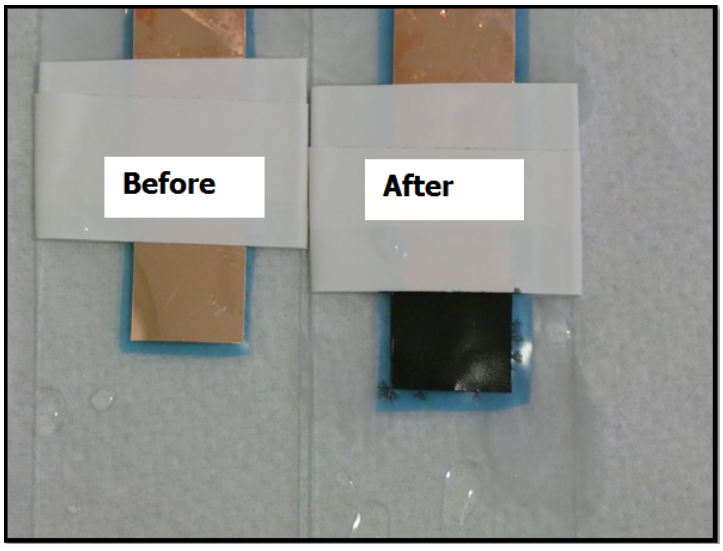

Figure 3.1: The electrodeposited 3DPNi substrate. The black layer is the porous Ni layer.

3.1.1. Structure and morphology

The type of Ni deposited in this case is called ”black” nickel, as is clear from the colour of the deposit. It is generally used for solar collectors and decorative processes. This is characteristic of deposition

from nickel sulphate solutions.[57]. Due to the random generation of H_2 bubbles at the working electrode, the nickel deposit forms a porous self-supported 3D structure. The metal deposit has a distinct cauliflower-like morphology. The structure is characterized by homogeneously distributed pores connected by network of nanostructured walls. The pore sizes range from the micro to nano size regime. The pores at the surfaces are typically larger (~5-20 µm) than the ones towards the bottom of the deposit. This can be explained by the behaviour of the H_2 bubbles to coalesce as they move to the upper surface of the deposit[45].

The deposit morphology is dependent on the dynamics of the diffusion layer along the working electrode surface area, which changes rapidly as the time progresses. In this case, with high current density, both the H_2 gas detachment from the Cu surface and the electroconvection (flow of molecules of a liquid crystal under the influence of an applied electric field) process are the deciding factors of the thickness and morphology of the layer[46]

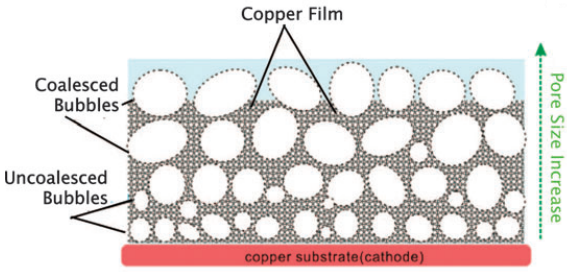

Figure 3.2: Mechanism of H_2 bubble coalescence. [45]

The walls of the 3D network are composed of Ni nanoparticles of sizes ~50 - 300 nm. There are numerous pores of sizes less than 100 nm between these particles. The micropores combined with the inter-nanoparticle spacing reveal the extreme porosity of the sample. This also suggests that it will be able to accommodate volume changes during Li cycling as well as offer an enhanced area for Li deposition.

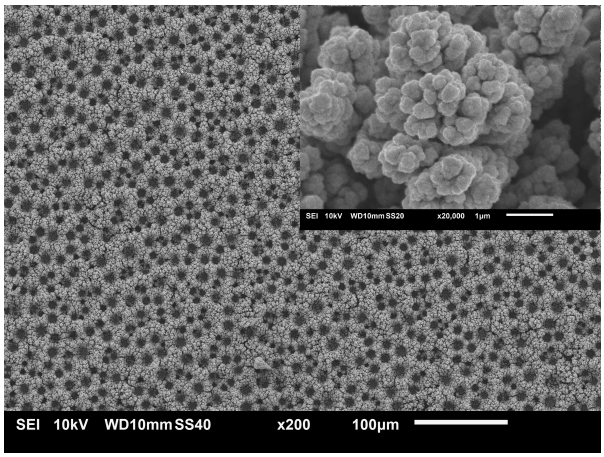

Figure 3.3: SEM image of the 3DPNi deposit on copper foil. The inset shows a magnified image of the Ni nanoparticles.

The thickness of the deposit is proportional to the duration of deposition. A deposition time of 30s yields a deposit of thickness ~30 µm and a 60s deposition gives a deposit thickness of ~50-60 µm. The deposit has inter-connected dendritic structures with quasi-cylindrical pores between them.

However, the two parameters, thickness and duration of deposition do not have a linear relationship since the electrochemically active surface area available for deposition varies with time. Initially (at time t = 0) the area available is equal to the area of Cu foil (1 cm^2). As time progresses the area available changes rapidly due to the deposition of the Ni. This also alters the current density of deposition. The area available for electrodeposition increases with the growth of the porous 3D Ni structure. Therefore, the current density of deposition at the working electrode reduces as the time progresses.

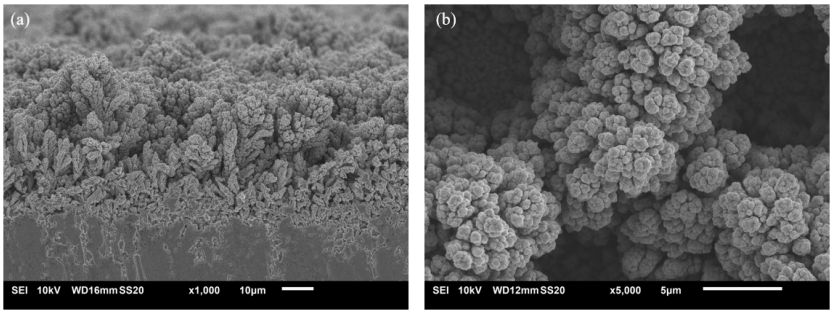

Figure 3.4: (a) Cross-sectional image of the deposit with 60s deposition. (b) Network walls of the 3D structure with the Ni particles.

The XRD and EDS spectrum of the deposit gives an insight into the metallic nature of substrate. The XRD spectrum show signals from both Cu and Ni as expected. The peak positions confirm poly-crystalline metallic nature of the deposit. The EDS data shows that there are no extraneous deposits formed, like nickel oxide or nickel hydroxide

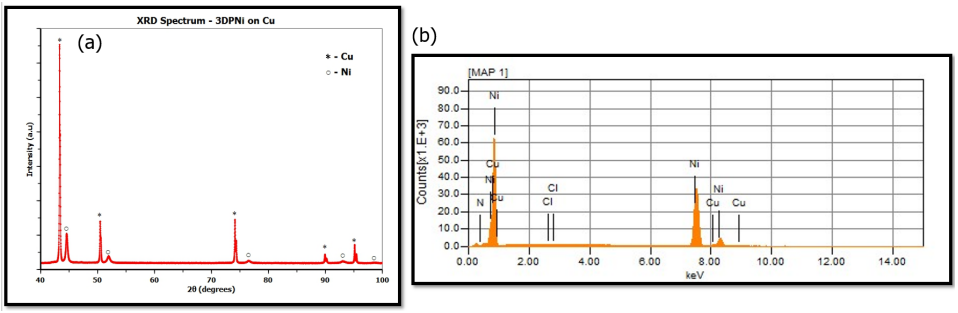

Figure 3.5: (a) XRD and (b) EDS spectra of the 3DPNi deposit.

3.1.2. Porosity

The amount of Ni deposited was calculated by weighing the sample before and after (with sufficient time for drying) the deposition. The mass loading was found out to be ~5 mg·cm^{-2}. It is important to calculate the current efficiency (Faradaic efficiency) of this process. It can be defined as the ratio of the actual mass of a substance deposited from an electrolyte to the theoretical mass deposited as predicted by the the Faraday's law of electrolysis. According to the law, the weight of the metal deposited in grams is,

$$W = \frac{ItA}{nF} \tag{3.1}$$

where W = weight of plated metal (g), I = deposition current (A), t = time (s), A = atomic weight of the metal (g/mol), n = valency of the dissolved metal in solution, Faraday's constant F = 96,485.309 (C/mol). The theoretically predicted weight of metal plated using this equation with I = 3A and t = 30s, gives us W = 27.3 mg. The Faradaic efficiency (η) then can be calculated as,

$$\eta = \frac{5}{27.3} = 0.183 = 18.3\% \tag{3.2}$$

This low efficiency can be attributed to the fact that a significant amount of current is used in reducing the H^+ ions in the electrolyte to H_2 gas. This low efficiency leads to the high porosity. Using the theoretically and experimentally measured mass, we can arrive at a practical value of the porosity of the substrate. The porosity (Φ) of the sample can be calculated as,

$$\Phi = \frac{V_p}{V_t} = 1 - \frac{V_{deposit}}{V_t} = 1 - \frac{m_{deposit}}{m_t} = 1 - \frac{5}{27.3} = 81.7\% \tag{3.3}$$

where, V_P is the pore volume, V_t is the total volume of the sample, $V_{deposit}$ is the volume of the deposit, $m_{deposit}$ is the mass of the deposit and m_t is the theoretical mass deposited. Thus, we get a porosity higher than 80%. Thus, the HBDT method is an effective way of producing porous structures. Even though the HBDT method does not rank high in terms of the efficiency, it is an effective method to produce thick 3D porous structures in a facile, simple, one-step and fast process. Another major advantage of the HBDT process is the fact that it offers a variety of parameters that can be modified to give an enhanced control of the composition, structure and morphology of the deposit. Some of the factors that affect the nature of the deposit are:

1. Current density & duration of deposition
2. Electrolyte bath composition
3. Distance between the electrodes
4. Electrode surface modification
5. Orientation of the electrode
6. Temperature of deposition
7. Agitation of the electrolyte bath

As mentioned before, the electrolyte bath composition (addition of PEG), the current density and duration of deposition were modified to obtain substrates with different structure and morphology. Finding an optimized structure as an anode scaffold for Li (or Na) is beyond the scope of this work. The parameters were altered to prove that different variations of the 3DPNi structure can be used for this purpose and that there is a possibility of finding an optimized structure with further research.

3.1.3. Effect of electrodeposition parameters - Structure & Morphology

Surfactant concentration - PEG is a surfactant that can be used to reduce the surface tension between the air-liquid (H_2 - Electrolyte) interface in order to impede the coalescence of the bubble. As mentioned previously, PEG is also a common additive in copper electrodeposition process. PEG is insulating in nature and it reduces the conductivity of the electrolyte and drives up the potential of the plating process. This makes the electrodeposition process harder. Both these combined effects results in a deposit with smaller Ni grains and smaller pore sizes. The approximate range of PEG to be used for this experiment was determined from the literature[48][58]. The different PEG concentrations tried were 0, 100, 150, 200 and 500 mg per 300 ml of water. The current density of deposition was 3 $A{\cdot}cm^{-2}$ and the duration of deposition was 30s.

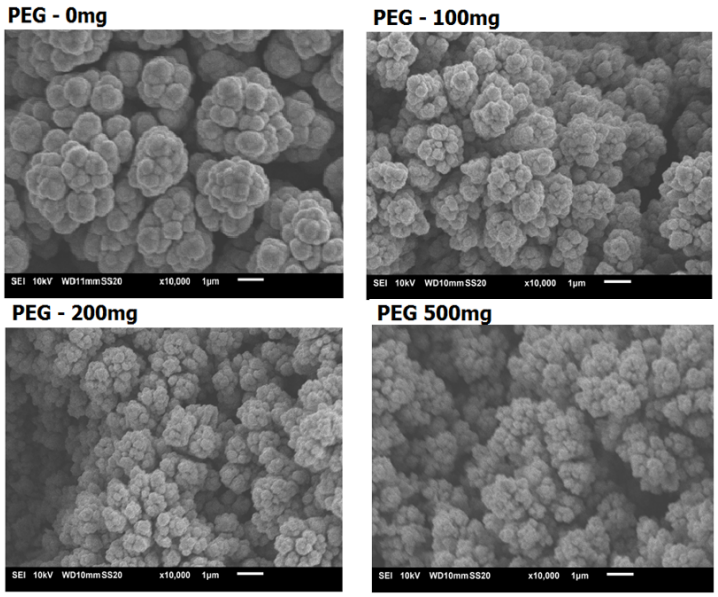

Figure 3.6: Comparison of the sizes of Ni grains with different amounts of PEG.

It is evident from the figures (3.6 and 3.7) that addition of PEG profoundly affects the structure and morphology of the deposits. We can see that adding PEG reduces the Ni grain sizes. The smaller

deposits may be attributed to the smaller H_2 bubbles as well as brightening effect of PEG, which disperses the Ni deposits over the substrate resulting in the formation of smaller grains[48]. From a physical sense, formation of smaller bubbles by preventing them from coalescing, results in reduced space between the bubbles for the Ni to deposit. The smaller spaces between the bubbles ultimately results in smaller deposits. While it is hard to quantitatively comment on the roughness variations with different PEG concentrations, it can be assumed that the addition of PEG does indeed make the 3DPNi rougher in nature as can be seen from the figure below. Also, the porosity of the substrate has also increased markedly.

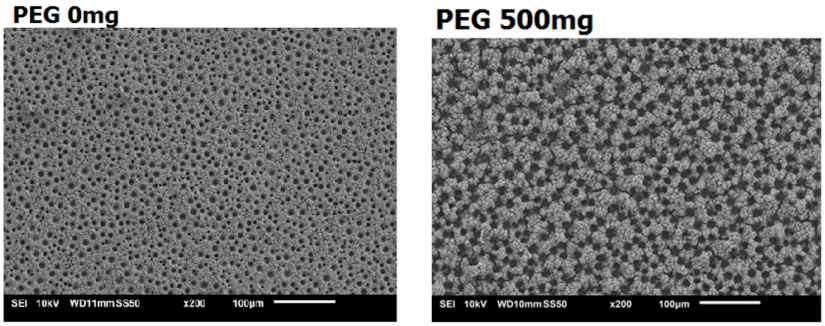

Figure 3.7: Top-view of the 3DPNi substrate fabricated without (0 mg) PEG and with (500 mg) PEG.

Current density - 3DPNi substrates were also fabricated with different current densities - 1, 3 and 5 $A{\cdot}cm^{-2}$. As discussed previously the current density of deposition affects the amount of H_2 bubbles created during the deposition process. Increasing the current density yields a more porous structure. However, it was found that this comes at the expense of the mechanical stability of the Ni structure. The vigorous formation of bubbles and the subsequent disturbance of the electrolyte near the working electrode will have a detrimental impact on the stability of metal deposition. Ni deposits were observed to peel-off from the working electrode at 5 $A{\cdot}cm^{-2}$ although the 3DPNi structure after deposition was still intact.

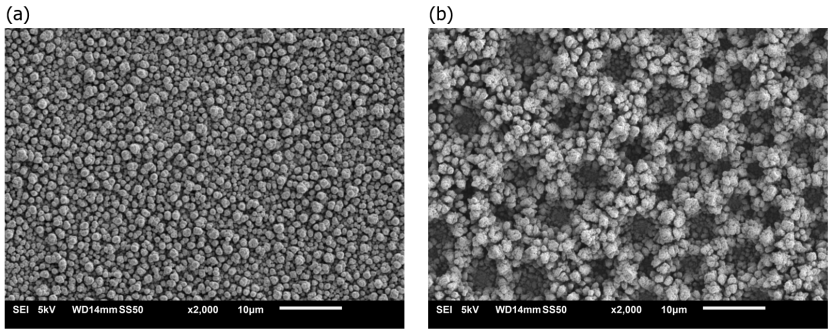

Figure 3.8: Top-view of the 3DPNi substrate fabricated with (a) 1 $A{\cdot}cm^{-2}$ and with (b) 3 $A{\cdot}cm^{-2}$

The potential of plating increases as we increase the current density. For a 3 $A{\cdot}cm^{-2}$ deposition, the range of potential values was between 14-17 V. The potential of plating was also directly proportional to the PEG concentration as mentioned before. In principle, increasing the current density will give structures with higher porosity, however at the the expense of mechanical integrity.

Duration of deposition - As discussed in the earlier section, the duration of deposition controls the thickness of the deposit. However, it was noted that with increasing deposition time (>80s), the Ni particles were seen to fall-off from the deposit. Therefore, as the deposit grows thicker with time, the Ni deposit towards the surface do not adhere well to the 3D structure due to vigorous stirring action by the H_2 bubbles. This causes it to peel-off as seen in the case with high current density of deposition. However, it might be possible to overcome this by changing the orientation of the electrode or changing the electrolyte bath composition.

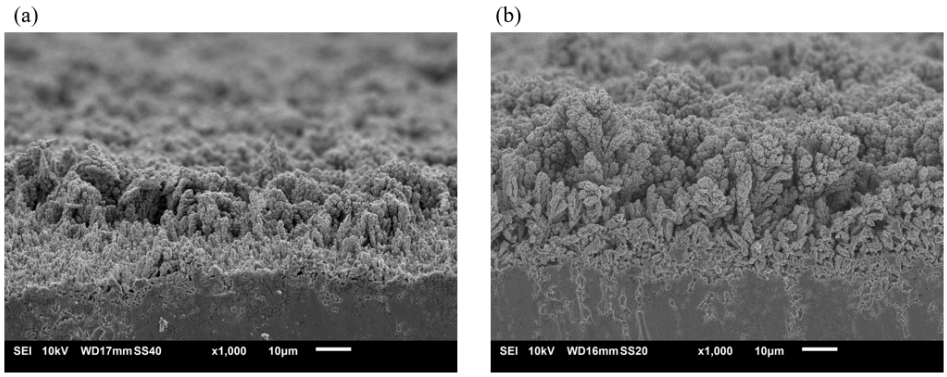

Figure 3.9: 3DPNi substrates with (a) 30s deposition (b) 60s deposition. The Cu substrate can also be seen underneath the Ni deposit.

3.2. Electrochemical Li cycling

3.2.1. Potential and Coulombic efficiency of Li cycling

The primary aim of this work is to determine if the 3DPNi substrate can effectively cycle Li i.e have Li^+ ions plated (deposited) as Li metal on the substrate and then stripped (removed) from it for a long period of time without failure.

1. Plating: $Li^+ + e^- \rightarrow Li$
2. Stripping: $Li \rightarrow Li^+ + e^-$

Hence, to understand the results of the Li (and Na) cycling in the symmetric cell (see figure 2.2), it is important to understand the basics of electrochemical Li cycling. Two important parameters pertinent to the process are:

1. Potential of Li cycling - Each of the plating and stripping process has an electric potential (voltage) associated with it. However in reality, the processes do not occur at the thermodynamically predicted value due to kinetic limitations of the reactions and the polarization effects. The difference between this theoretically determined potential of a half reaction (plating or stripping) and the experimental observed one is termed as the overpotential. The thermodynamic potential of the Li plating and stripping process is 0 V, since the relative potential of both the electrodes is zero. The deviation from this value (0 V) during the plating and stripping process is the overpotential of Li cycling. The following figure is the voltage-time plot for one complete Li cycling process. The plating process has a negative voltage and the stripping process has a positive voltage value. The overpotential in this case is the difference the two potentials. The term voltage hysteresis is also used to denote overpotential. Since the Li cycling process is done under galvanostatic conditions, the time axis maybe directly converted to capacity by multiplying the current density.

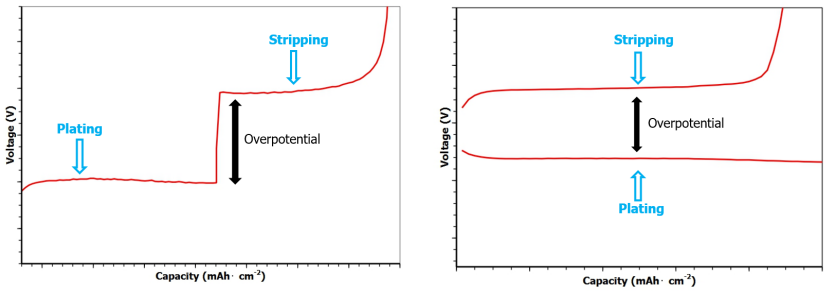

Figure 3.10: Typical voltage-time plots of one Li cycling process. Both the graphs represent the same process.

2. Coulombic efficiency - The Coulombic efficiency is defined as the ratio of the stripping capacity to the plating capacity. The plating (discharge) capacity is the amount of Li^+ ions deposited

on the 3DPNi substrate from the Li metal foil (counter electrode). This value remains constant throughout the cycling process since the Li metal is an infinite source of Li atoms. The stripping (charge) capacity is the amount of Li that can be removed from the 3DPNi substrate in the following stripping process. Both capacities are expressed in terms of $mAh \cdot cm^{-2}$. The area of the 3DPNi substrate used throughout the work is $1cm^2$.

3.2.2. Cycling with different 3DPNi substrates

To study the performance of substrates fabricated with different amount of PEG (100, 150, 200 and 500 mg), it was subjected to Li cycling in a symmetric cell. The capacity of deposition was chosen to be 0.5 $mAh \cdot cm^{-2}$. The cell was cycled at a rate of 1 $mA \cdot cm^{-2}$, i.e one cycle of Li plating and stripping would take 1 hour. Figure 3.8 shows a comparison of the Coulombic efficiency of the 3DPNi substrates and the reference foil. As is evident from the figure, the 3DPNi substrates show a higher average Coulombic efficiency for much longer duration of time as compared to the reference copper foil.

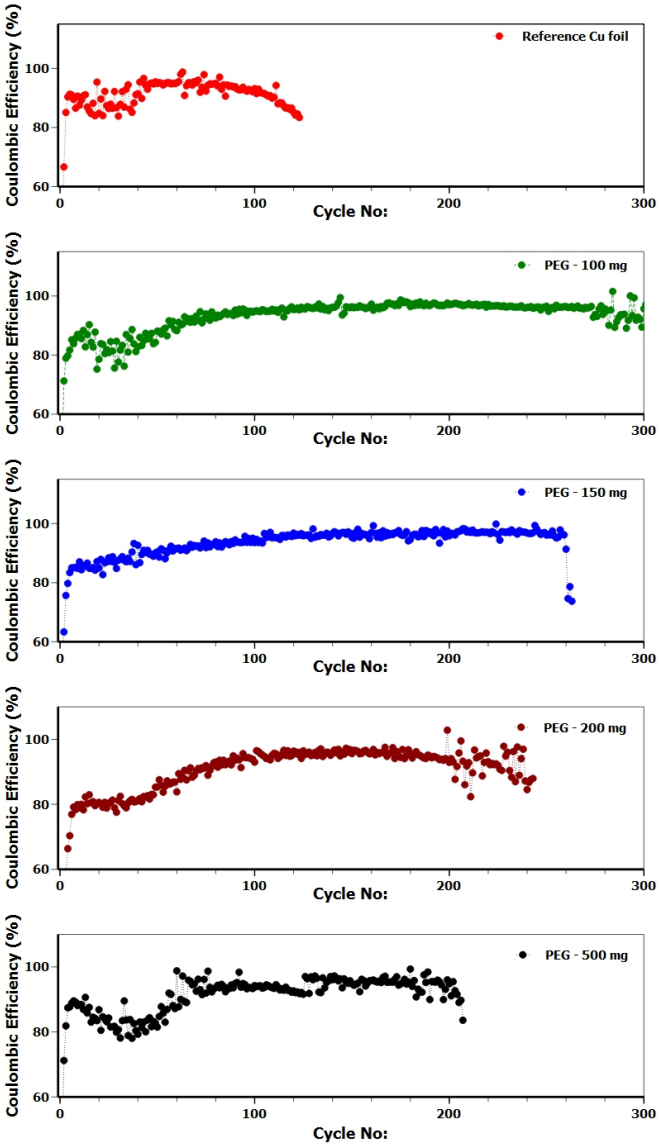

Figure 3.11: Coulombic efficiency of 3DPNi substrates fabricated with different amounts of PEG & reference Cu foil

The average performances of the various 3DPNi substrates can be summarized as follows:

1. Reference Cu foil = ~ 90% efficiency for 120 cycles
2. PEG - 100mg = ~ 93% efficiency for 300 cycles
3. PEG - 150mg = ~ 93% efficiency for 260 cycles
4. PEG - 200mg = ~ 90% efficiency for 240 cycles
5. PEG - 500mg = ~ 91% efficiency for 200 cycles

The cells were stopped once the charging capacity began fluctuating and the efficiency went below 70-80%. Or when it was shorted (i.e 0 V) (see appendix for failure modes). It is clear that 3DPNi substrates fabricated through the HBDT method is a viable option for Li metal anodes. However, the Li cycling behaviour deserves a closer look.

A common trait of all the five plots is the exceptionally low (~30-40%) Coulombic efficiency for the first cycle. This can be attributed to the SEI formation (see section 1.2.4). During the first cycle, the Li^+ interacts with the anionic species in the electrolyte and forms a layer of SEI on the 3D Ni surface. This irreversible process consumes a high amount of Li (supplied by the counter electrode) and hence it leads to the low efficiency. This process continues as long as the SEI layer is stabilized. It can also be seen that reference Cu foil has a higher efficiency in the initial stages. This is because of its smaller surface area. The increased surface area of the 3DPNi leads to the formation of the larger SEI layer and this involves higher amount of irreversible Li^+ consumption. Once the layer is formed and the system is stabilized, the efficiency starts to grow.

All the four graphs pertaining to the 3DPNi substrate, show a characteristic dip in the efficiency before it climbs to ~100%. This forces us to consider that there is another mechanism at play here. A possible reason may be nano-porosity and roughness of the 3DPNi substrate. As is clear from the SEM images, the 3DPNi substrate is interspersed with both micro and nano-sized pores. The nanopores are distributed randomly with no size or shape correlation. The Li plating (and stripping) will be significantly harder in these nanopores (and other nanosized voids) as compared to the micropores. The plating and stripping will also depend on the accessibility of these nanopores to the electrolyte. Hence, it may be theorized that the dip in efficiency may be due to the excessive roughness of the sample and the filling of these nanopores. Once these nanometer sized voids are filled, the Coulombic efficiency picks up again and the cycling process happens in a uniform manner. However, more experiments needs to be done to confirm this.

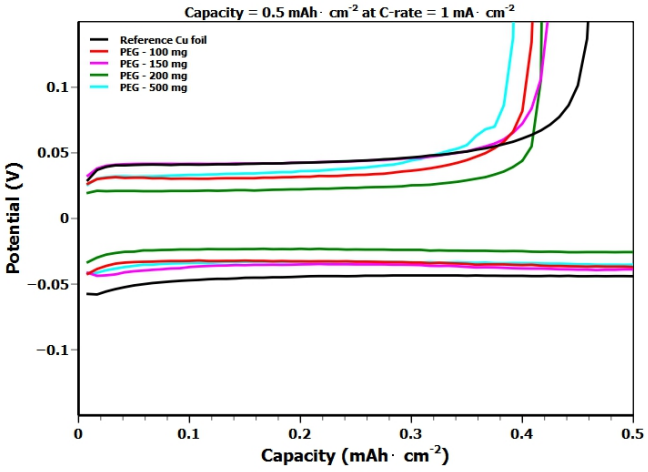

Figure 3.12: The voltage profiles of the plating and stripping processes after 50 cycles for 3DPNi substrate fabricated with different PEG concentrations.

It is important to see the voltage-capacity plot as well. The voltage hysteresis of the curve offers another yardstick to measure the Li cycling process. Ideally, the voltage hysteresis should be minimum and should not be subject to too much variations. The plating process is represented by the line in the negative portion of the y-axis and the stripping process by the positive portion. We can also see that all the 3DPNi substrates used, show a lower voltage hysteresis than the Cu foil.

Another interesting aspect of the voltage-capacity plot is that the it does not follow any trend. The substrate fabricated with PEG mass of 200 mg shows the lowest voltage hysteresis, with the substrate with 100 mg PEG coming next. It is then followed by substrate made from PEG mass of 500 mg while the PEG 150 mg version has the highest hysteresis. It could be expected the substrate fabricated with 500 mg PEG might have the highest potentials since it is expected to have the highest area.However, this is not the case. This tells us that the area-potential relationship is not a straight-forward one. Another porbable reason might be that all the surfaces are not wetted equally by the electrolyte.

From both the Coulombic efficiency and voltage-time curves, it was decided that PEG concentration of 100 mg per 300 ml of H_2O would be best suited to fabricate substrates for further studies. Following this, 3DPNi substrates were also prepared with different current density and duration of deposition.

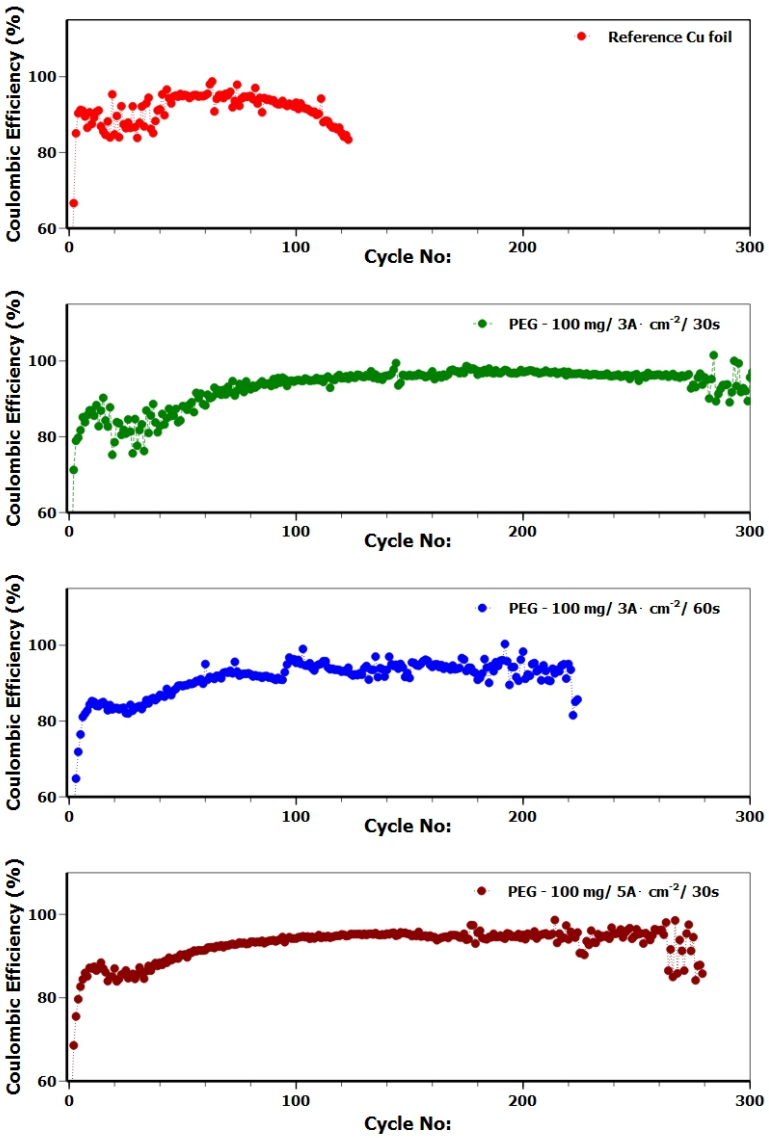

Figure 3.13: Coulombic efficiency of 3DPNi substrates fabricated with different current densities of deposition & reference Cu foil

The above plots tells us that the earlier configuration - PEG 100 mg, current density of 3 $A \cdot cm^{-2}$ and 30s deposition still shows superior performance over the variations. However, the capacity and current rate of Li cycling plays a very significant role in deciding what porosity and thickness would give the best performance. Therefore, it must be understood that the performance of the substrate

will be dependent on the capacity and c-rate and the 100 mg/ 3 A·cm^{-2}/30s substrate might be best performing one in this specific case. Anyhow, this configuration was chosen to continue the studies.

3.2.3. Study of Li cycling performance

Different capacity - Constant current rate - To further probe the performance of the substrate, different capacities of Li were cycled with the substrate. The current rate of cycling was kept constant at 1 mA·cm^{-2}.

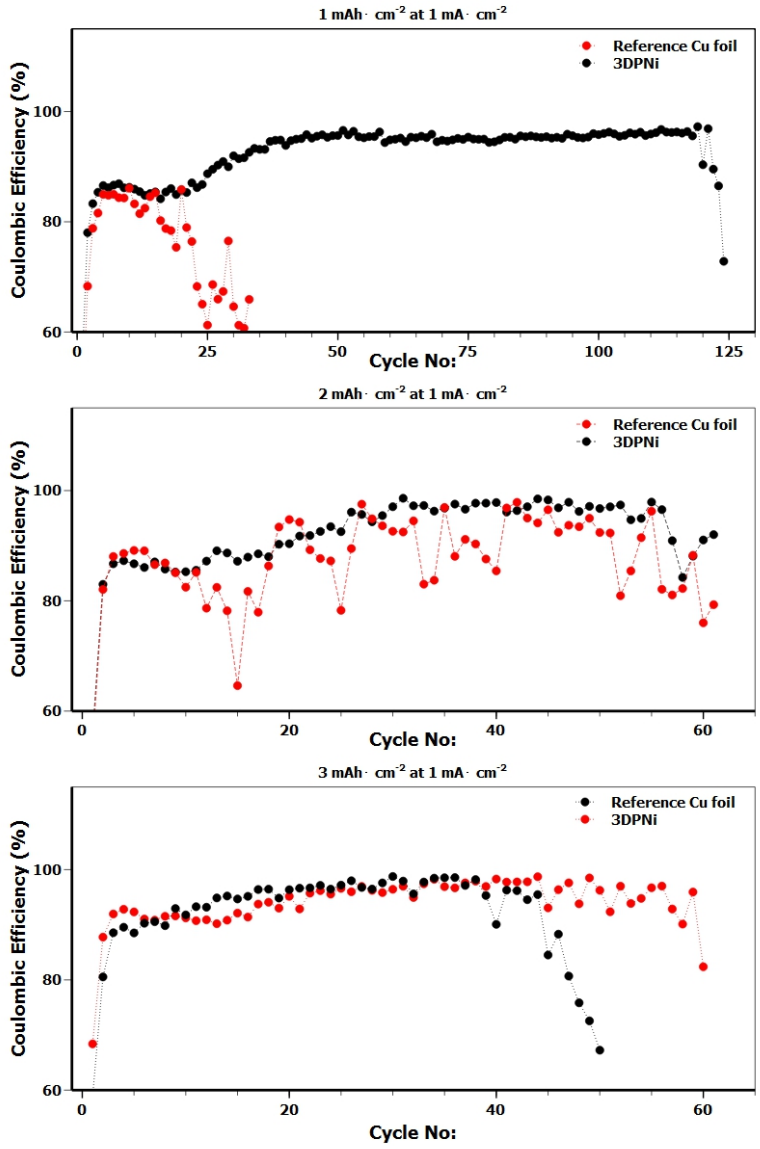

Figure 3.14: Coulombic efficiency of 3DPNi substrates cycled with different capacities of Li.

It is clear that the 3DPNi shows better Coulombic efficiency than the Cu foil. However, the cycle-life of the substrates reduces as the capacity increases. As the amount of Li cycled in the substrate increases it exerts more stress on the substrate, this reduces its cycle life. The average Coulombic efficiency of the substrates at different capacities are as follows:

1. 1 mAh·cm^{-2} = ~ 92% efficiency for 120 cycles
2. 2 mAh·cm^{-2} = ~ 92% efficiency for 65 cycles
3. 3 mAh·cm^{-2} = ~ 94% efficiency for 60 cycles

The 3DPNi substrate shows a relatively good cycling performance when the capacity is limited 1 mAh·cm^{-2}. However, there is a significant drop in performance when the capacity is increased. This may be due to the fact that 30s deposition might not be thick enough to accommodate the large capacity. Therefore, understanding the capacity-thickness relation of the 3DPNi substrate will be a key step in improving the performance of the substrate. More study has to be done in the direction of investigating the Li nucleation thermodynamics and kinetics. The work by *Pei et al.* published in January 2017 gives more insight into this field[59]. The study here is done for Li cycling with planar Cu substrates. It can be safely assumed that this behaviour will be different on a nanostructured 3D structure. Also, the potential of Li nucleation will also vary among different metals. This calls for a much detailed foray into this field.

Kinetics - The earlier electrochemistry experiments demonstrate that the Coulombic efficiency for the initial 20 odd cycles are relatively low (<90%). The low efficiency may be due to any of the three following reasons:

1. Irreversible SEI formation
2. 3DPNi substrate
3. Li^+ kinetics of diffusion

Among this, the irreversible SEI formation is a spontaneous process that stabilizes as the cycling progresses. This raised the suspicion as to whether the 3D structure of the 3DPNi substrate or the intrinsic kinetics of Li^+ ion transport was responsible for this low efficiency. In an earlier section (section 3.2.2, page 25) it was also hypothesized that it could be the structure-morphology characteristics of the substrate that might be contributing to the low Coulombic efficiency.

To investigate this issue, the kinetic aspects of the Li^+ ion was studied by reducing the current rate of the Li cycling after every 20 cycle. The current rate was fixed at 1 mA·cm^{-2} for 20 cycles and for the next cycle the current rate was reduced to 0.1 mA·cm^{-2} for the next cycle. The cut-off voltage for charging in these tests was limited to 0.5 V. If we observe a dramatic increase in Coulombic efficiency for every 21st cycle, then we can conclude that cycling the Li^+ ions at a slower rate can extract (strip away) a high amount of the previously plated Li.

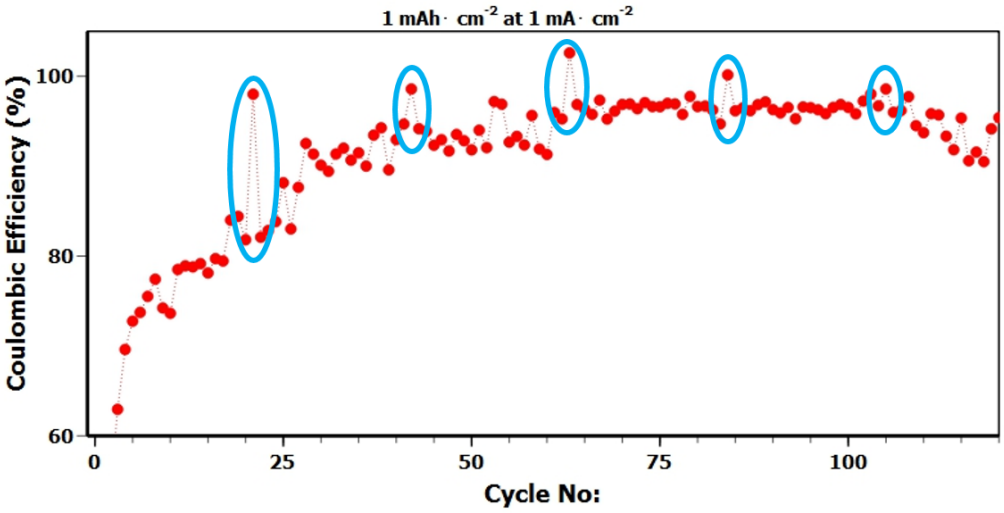

Figure 3.15: Coulombic efficiency of 3DPNi substrate cycles at 1 mA·cm^{-2} for 20 cycles and 0.1 mA·cm^{-2} for the next cycle. The highlighted portion shows the jump in efficiency.

The result shows that for every 21st cycle, there is a dramatic increase in the efficiency. This is highlighted in the graph. Therefore, if we strip the Li from the 3DPNi in a sufficiently slow manner, we can reach efficiency of almost 100% (i.e at a reduced rate of 0.1 mA·cm^{-2} the Li is able to strip away from the 3DPNi substrate effectively). This confirms that the limitations from the Li^+ diffusion characteristics combined with the irreversible capacity loss due to the SEI formation is responsible for the loss of Coulombic efficiency in this case. The 3DPNi substrate does not impede the Li plating and stripping process.

3.3. Electrolyte modification with $LiNO_3$

The normal electrolyte was modified with the addition of 1 wt% $LiNO_3$. The $LiNO_3$ addition impacts the Li cycling by the formation of a stable passivation layer on the electrode surface. The surface layer is composed of species of the form Li_xNO_y formed due to the reduction of $LiNO_3$. This layer further homogenizes the SEI layer formed and enables the electrode to reach high Coulombic efficiency values from an early stage[60]. The effect of $LiNO_3$ addition on the initial efficiency can be clearly understood by comparing the 3DPNi substrates cycled for 5 times with and without $LiNO_3$.

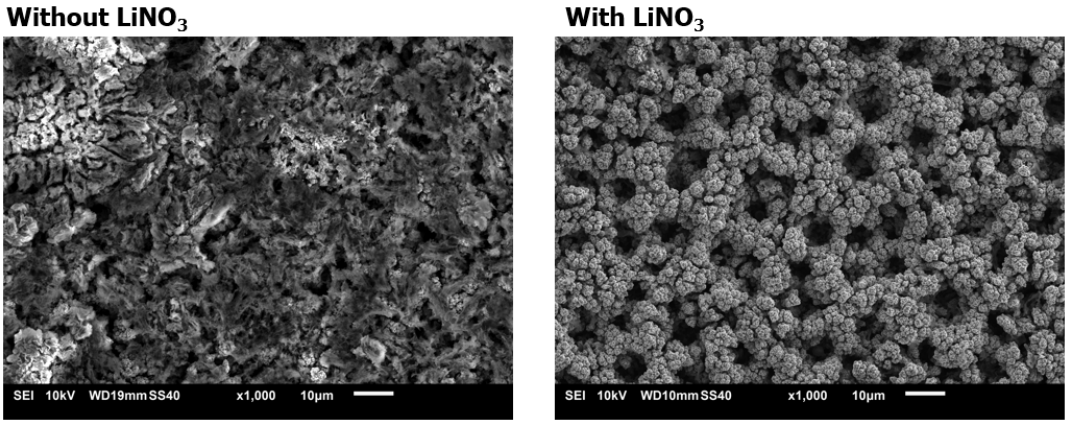

Figure 3.16: Effect of $LiNO_3$ addition. Both the 3DPNi substrates were cycled for 5 times with a capacity of 1 $mAh{\cdot}cm^{-2}$ at 1 $mA{\cdot}cm^{-2}$.

The image above illustrates the stark contrast that arises due to the $LiNO_3$ addition. It can be seen that with the normal electrolyte there are a lot of artifacts due to the Li cycling process due to the stabilization of SEI. These artifacts offer higher resistance and longer distance for Li^+ ion transport. However, with the addition of $LiNO_3$, the formation of passivation layer enables the Li to be cycled with close to 100% efficiency from the first cycle.

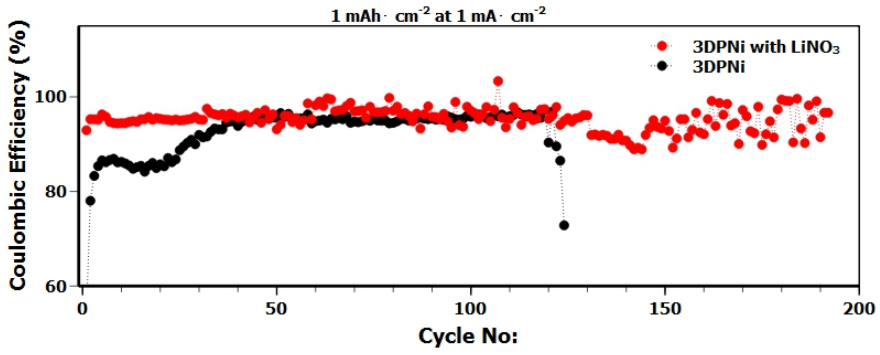

Figure 3.17: Coulombic efficiency of 3DPNi substrate using the electrolyte with and without $LiNO_3$ addition.

The addition significantly improved the Coulombic efficiency of the Li cycling process as expected. There is a dramatic increase in the Coulombic efficiency of the first cycle. By adding $LiNO_3$ to the electrolyte, the efficiency reaches almost 93% whereas without $LiNO_3$, the efficiency drops to less than 80%. This indicates that the formation of the passivation layer is a spontaneous process. Also, the Li nucleation during this first cycle is a markedly different process. The Coulombic efficiency remains more than 95% close to 200 cycles with the addition $LiNO_3$ as compared to 92% for 120 cycles with the normal electrolyte.

This graph gives us two important conclusions:

1. The addition of $LiNO_3$ alters the potential of stripping for the initial cycles significantly. With

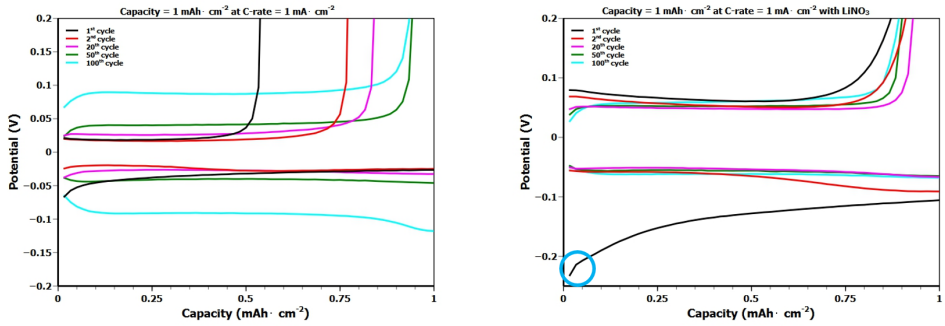

Figure 3.18: The voltage profile of the plating and stripping processes after 1, 2, 20, 50 and 100 cycles for 3DPNi substrate cycled with and without $LiNO_3$

$LiNO_3$, the Li plating for the first cycle happens at a voltage lower than -0.2 V (highlighted with the circle) as compared to ~0.06 V for the normal electrolyte. This dip is due to the larger interfacial resistance in the case of $LiNO_3$. This tells us that there is no electrochemical reaction before the first plating.

2. In the $LiNO_3$ case, the hysteresis tends to remain constant after the initial cycles. There is minimal variation between the potential of plating and stripping for the 20^{th}, 50^{th} and the 100^{th}. This shows the formation of the passivation layer which stabilizes the Li cycling process and enables it to retain its high Coulombic efficiency for higher period of time. This is not so in the case without $LiNO_3$. The voltage hysteresis increases gradually as the cycling progresses. It can also seen that the capacity of stripping also increases along with this. The voltage hysteresis reaches up to 0.18 V for the 100^{th} cycle, while it is less than 0.1 V with $LiNO_3$. This gradual increase in the voltage hysteresis may be attributed to the increasing thickness of the interphase layer which impedes the plating-stripping process. However, we must also consider the probability of electrolyte decomposition in some cases. This conclusion may apply to either case since the electrolyte decomposition may happen due to various external factors as well[29].

The Li nucleation characteristics and the voltage hysteresis behaviour is reflected in the EIS results as well.

3.4. Electrochemical Impedance Spectroscopy

The EIS analysis was done on the reference Cu foil and the 3DPNi substrate, with the normal electrolyte and with $LiNO_3$ addition.

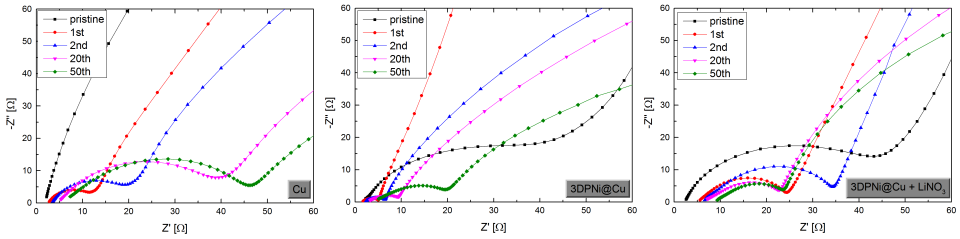

Figure 3.19: EIS results of the different 3DPNi substrates and the reference copper foil

The EIS behaviour of the system resembles that of the mixed kinetic and charge transfer control model as shown in figure 2.4. Therefore, by comparing the results to the standard graph we can analyze the impedance characteristics of the cell.

The solution resistance of all the three systems are comparable (less than 10 Ω). However, with the addition of $LiNO_3$ the resistance value increases slightly as compared to the other two cases. Considering the charge transfer resistance the reference Cu foil, it has a much higher value than the 3DPNi substrate in the case of pristine substrates. This tells us that the conductive 3D Ni structure with larger surface area enables easier charge transport within the cell. Comparing the normal electrolyte with the $LiNO_3$ added one, we see that $LiNO_3$ addition increases the charge transfer resistance significantly.

This confirms the presence of the passivation layer formed with the Li_xNO_y species which impedes the charge transfer process.

Another aspect of note, is that for the substrate with $LiNO_3$ the charge transfer resistance saturates to around 25 Ωafter the first cycle. In the case of normal electrolyte, the charge transfer resistance increases in a steady manner. The additional passivation layer formed with the Li_xNO_y species stabilizes the charge transfer process. However, this happens at the expense of increasing the charge transfer resistance. This is contrary to what we see in the case of normal electrolyte, in whose case the the impedance curve (charge transfer resistance) increases progressively. This can be explained by the increase of the SEI layer thickness as the cycling continues. The fact that we do not see this behaviour in the case of $LiNO_3$ addition leads us to believe that as the cycling progresses, the passivation and the SEI layer stabilize the environment and offer the same charge transport resistance to the Li^+ transport. In other words, there is no further irreversible loss of Li through the SEI formation. This claim is supported by the voltage hysteresis plot as well (see figure 3.16).

3.5. Structure & surface characterization of cycled substrates

To investigate the structural and morphological changes in the 3DPNi substrate at various stages of cycling, symmetric cells with 1 mAh·cm^{-2} capacity were cycled at a current rate of 1 mA·cm^{-2} for 1, 2, 5 and 50 cycles. The effect of the base electrolyte and the $LiNO_3$ addition were studied. The cells were then dismantled and the substrates were studied with SEM.

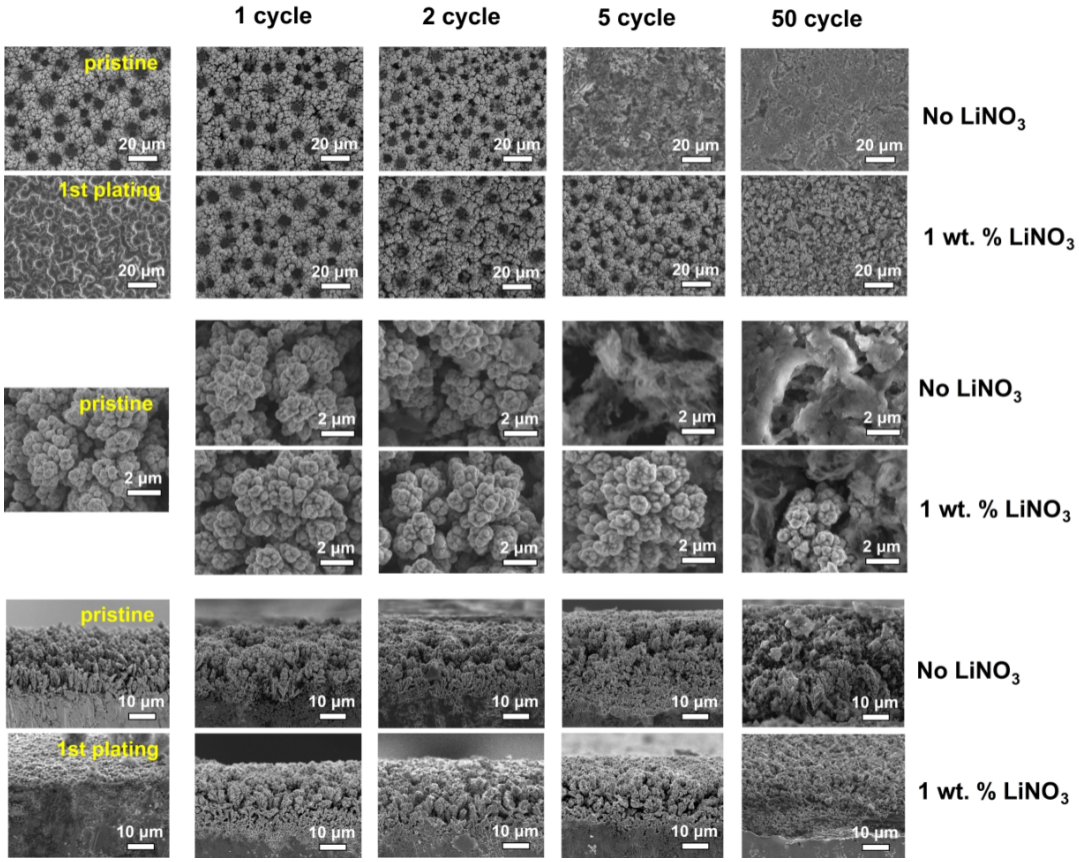

Figure 3.20: SEM images of the 3DPNi at different stages of cycling with & without $LiNO_3$

The SEM images support the findings of the voltage profile and EIS results. The first two rows shows the top-view of the substrates. The image of the '1st plating' tells us that the Li can be effectively contained in the 3DPNi structure. 3 mAh·cm^{-2} of Li was deposited on to the sample to study if Li could be effectively contained in the 3D structure. The image shows us that the Li plating happens effectively with the structure and the Ni shows good affinity to the Li. This also suggests a good wetting of the substrate by the electrolyte.The images towards the right, tells us that the structure is

mechanically stable even after 50 cycles in both cases. However, there is significant difference in the cycling behaviour in each case. After the 1st cycle, the 3DPNi looks comparable to the pristine structure but for the substrate without $LiNO_3$ addition, the network walls have become thicker than the one with $LiNO_3$ addition. This points to irreversible SEI formation as well as the stray Li deposit which could not stripped off effectively. The 5th cycle images gives a much clearer indication of the difference between the effects of the two electrolyte systems. It is clear that the addition of $LiNO_3$ greatly enhances the Coulombic efficiency, as is clear from the amount of free space in the substrate. The structure also retains its shape and morphology. However, for the normal electrolyte, the substrate is covered in a layer of SEI artifacts and other Li deposits. This might not necessarily lead to failure of the substrate but just confirms the claim of homogeneous SEI layer formation in the case of $LiNO_3$ addition. This homogeneous layer results in a highly reversible Li cycling process. After 50 cycles, the amount of free space in both the substrates have reduced drastically. This is because of the interphase layer growing in thickness and the accumulated Li deposits which could not be stripped away after every cycle. Both these factors lead to reduced cycling efficiency. Even at this point, some of the cauliflower-like structure of the 3PDNi substrate is visible in the case of $LiNO_3$. While this proves beyond doubt that the 3D structure and morphology of the substrate is retained, it also forces us to believe that the SEI layer is formed predominantly on the top surface of the substrate. This especially true for the case without $LiNO_3$ addition because even though the SEM images shows the complete coverage of the top of the substrate with the SEI layer, the substrate under the same conditions can be cycled without failure for about ~120 cycles under the same conditions (see fig 3.10). These images also confirm that the structural integrity of the substrate is retained during the cycling process.

The 3rd and 4th row shows a magnified image of the individual 3DPNi substrate. This shows us that there is hardly any Li deposits in the nanopores between the Ni deposits in the first two cycles in both the cases. This questions the earlier claim that Li plating in nanopores is significantly harder and that might be the reason for the dip in the Coulombic efficiency. (section 3.2.2, page 22) The SEM images tells us that the initial dip in efficiency is solely due to irreversible consumption of Li due to the formation of the SEI. This is specially relevant in the case of normal electrolytes. The initial dip in the Coulombic efficiency could be due to the fact that the increased surface area of the substrate leads to the creation of a SEI layer with larger surface area compared to the planar substrate. Until the SEI formation is completed throughout the 3D structure and is stabilized, the Coulombic efficiency does not reach the stable maximum value. Even though the kinetics of the SEI formation is unclear, this theory is supported by both the SEM images and the Coulombic efficiency plots. However, more studies is required to understand the mechanism and kinetics of SEI formation. Continuing with this theory, it could also be argued that addition $LiNO_3$ expedites the formation and stabilization of the SEI layer at an enhanced rate. Since the SEI formation and stabilization happens at a faster rate, we do not see a drop in the Coulombic efficiency until the cell dies or short circuits.

3.6. Electrochemical Na cycling performance

Electrochemical cycling of the 3DPNi substrate with Na metal showed encouraging results. With the electrolyte system of $NaPF_6$ and DEGDME, Na could be cycled effectively with this substrate. Thus, the 3DPNi substrate can also reduce the dendrite formation in Na as well.

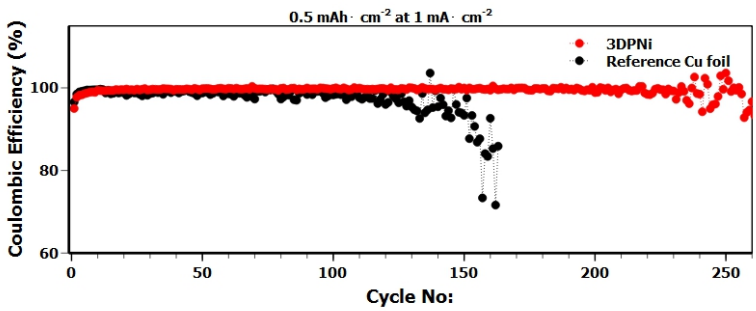

Figure 3.21: Coulombic efficiency of the Na metal cycling with the 3DPNi substrate and reference Cu foil.

The 3DPNi substrate gives an average performance of ~99% for more than 250 cycles. Even the Cu foil maintains more than 90% average efficiency for more than 150 cycles. This is significantly better than the Li cycling performance. However, attributing this superior performance solely to the 3DPNi substrate might not be a good conclusion. The fact that that both substrates show better performance than with Li tells us that is something inherently different with Na cycling. It could also be due to the particular electrolyte that was used for this experiment. This particular electrolyte was chosen from the work of *Seh et al.*. This work reports that The high reversibility was due to the formation of a uniform, inorganic SEI made of Na_2O and NaF, which is highly impermeable to electrolyte solvent and prevents the formation of dendrites[4].

This finding gives us optimism that similar to this case, there could also be an electrolyte system that improves the performance of Li metal cycling, without the other engineering innovations. It also highlights the importance of electrolyte system and the nature of SEI in metal cycling processes.

In any case, the superior cycling performance of Cu and 3DPNi substrates compared to that of Li leads us to believe that the Na cycling mechanism might be different from that of Li. The fast climb towards ~100% efficiency might be due to fast formation and stabilization of the SEI layer. This is similar in the case of both Cu and 3DPNi substrate which indicates that the SEI formation mechanism should be different fro Na. The electrolyte system used ($NaPF_6$ in DEGDME) might also be a defining parameter that affects the performance.

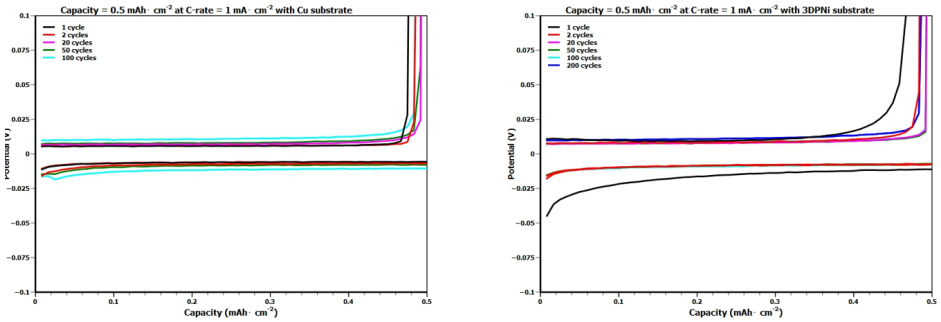

Figure 3.22: Voltage profiles of the plating & stripping processes of Na with Cu (left) and 3DPNi (right) substrate.

The voltage profiles of the Na metal cycling look vastly different from the case of Li. It is extremely stable through out the cycling progress and the voltage hysteresis is minimal. For the 3DPNi substrate the initial potential of plating is higher than that of the Cu substrate - it is almost -0.05 V as compared to the ~ 0.01 V of that of Cu. This may be due to the increased surface area and roughness of the 3DPNi substrate. The cycling process stabilizes soon after this. The voltage hysteresis of both the cases is around 0.03 V with the Cu substrate being on the lower side. This is the case even after 100 cycles and 200 cycles for Cu and 3DPNi respectively. Hence, it might be possible that the cell fails due to some other mode other than dendrite formation. This interesting behaviour definitely warrants further investigation.

3.7. Surface layer depositions

The ALD of TiO_2 and Al_2O_3 significantly improves the cycle life as well as the Coulombic efficiency of the Li cycling process. It is accepted to be due to the stabilization of the SEI layer, in an effect that is similar to the ceLiNO3 discussed before. However, the efficiency at the beginning of the both the depositions are low. It is around 50% for TiO_2 deposition and 35% for the Al_2O_3 case. This indicates a vastly different SEI formation/stabilization mechanism. The stabilization process is severely impeded by the deposition layer although, it shows superior performance once the stabilization process is completed. The slow rise of the Coulombic efficiency to the maximum tells us that the SEI stabilization process takes longer. The irreversible consumption of Li^+ ions in the early stages of cycling to stabilize the SEI results in the low Coulombic efficiency at the beginning. However, once the layer is formed and stabilized, the cycling behaviour is extremely uniform and long-lasting. Therefore, it is clear that surface layer deposition significantly alters the SEI formation mechanism and more study is needed to understand the various parameters affecting this process.

The voltage profile curves support our initial understanding. As can be seen, there is a significant

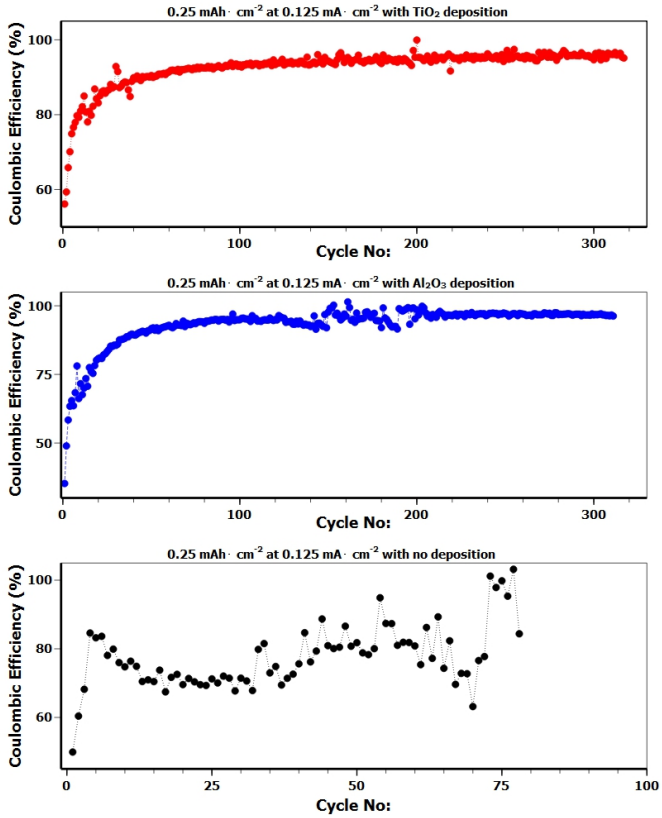

Figure 3.23: Coulombic Efficiency of the Ni substrate with Al_2O_3 and TiO_2 depositions compared to bare planar Ni foil.

loss of capacity in the initial cycles. However, this improves as the cycling progresses. Another interesting aspect that is common to both the cases is that the voltage hysteresis shows a decreasing trend till the 50^{th} cycle or so. It starts increasing between the 50^{th} and 100^{th} cycle. This increase in hysteresis keeps rising as time progresses. From a physical sense it means that the Li plating and stripping process is "easier" until 50^{th} cycle or so. So, the SEI formation and stabilization mechanism is significantly altered. This may be attributed to the SEI - ALD layer interaction but more experiments are required to have a more thorough understanding. Since, it is common to both the depositions, it can be definitely due to presence of the ALD layer, however, the reaction mechanism of both the cases should be different due to presence of different chemical species. This corroborated by the fact that in the case of TiO_2 the potential of plating is slightly more negative than in the Al_2O_3 case. Also, the voltage hysteresis is lower in the case of Al_2O_3 (~0.05 V) compared to TiO_2 (~0.07 V) after 300 cycles. Both these values are on the lower side compared to other cases.

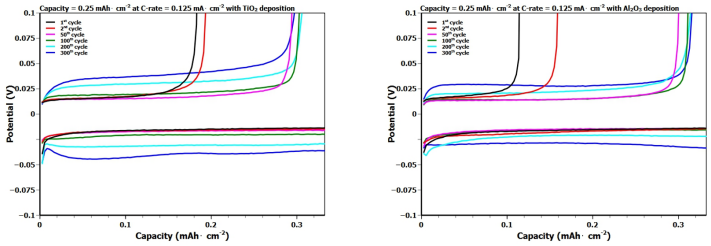

Figure 3.24: Voltage profiles of the plating & stripping processes of Li using substrates with TiO_2 (left) and Al_2O_3 (right) depositions.

The physical parameters of the ALD process like thickness of the layer, homogeneity, substrate -

layer interaction etc. will also play a significant role in deciding the Li cycling performance. The Li^+ ions need to traverse the SEI-ALD layer during both plating and stripping process therefore, how the layer forms (kinetics) and its chemical composition will be of utmost importance in this case. While most of that is beyond the scope of this project, it is confirmed beyond suspicion that ALD deposition indeed helps in delaying the dendrite formation and eventual failure of the battery.

4

Conclusions

4.1. Fabrication

The HBDT method is an effective, facile method to produce 3D metallic foam structures. Extremely porous structure with good mechanical integrity can be produced in minimal amount of time. The method also offers an option to modify numerous fabrication parameters and create structures with desired morphology and characteristics.

4.2. Li cycling experiments

The 3DPNi substrate is suitable as a conductive scaffold for Li metal anodes. It can function as a 3D current collector to reversibly store Li effectively. The results that have been obtained are comparable if not superior than the ones published in scientific literature. Using the 3DPNi electrode, the Li could be cycled for ~300 cycles at 0.5 $mAh \cdot cm^{-2}$ at $mA \cdot cm^{-2}$. Cycles lives of 120 and 60 cycles were achieved with capacity to 1 $mAh \cdot cm^{-2}$ and 3 $mAh \cdot cm^{-2}$ respectively at the same current rate. It was also proven that the 3D structure does not impede the diffusion behaviour of the Li^{+}.

4.3. Effect of $LiNO_3$

The addition of $LiNO_3$ significantly improves the Li cycling performance. As discussed before, the formation of the passivation layer is responsible for this effect. However, the nucleation and growth of this layer needs to be understood more clearly. The cycle life of the cell improved to more than 200 cycles at more than 90% efficiency with a capacity of 1 $mAh \cdot cm^{-2}$ at a current rate of 1 $mA \cdot cm^{-2}$. The voltage profiles of the two cases (with and without $LiNO_3$) are very different from each other. Addition of $LiNO_3$ makes the voltage hysteresis constant as the cycling progresses, while in the other case, the hysteresis increases gradually. Also, the initial Li plating potential is more negative in the case of $LiNO_3$, suggesting the formation of a passivation layer which results in the increase of Li plating potential.

4.4. EIS results

The EIS results clearly indicate that the 3DPNi substrate offers a much lower impedance to Li^{+} ion flux compared to the Cu foil. In the case of normal electrolyte, the impedance increases gradually as the cycling progresses. Addition of $LiNO_3$ increases the impedance of the cell. This is due to formation of the passivation layer. It causes the impedance to remain constant as the cycling progresses.

4.5. Structural Characterization

SEM imaging of the sample after various stages of cycling proved that the substrate morphology is retained even after 50 cycles. The electrolyte plays a significant role in deciding the cycling mechanism.

4.6. Na cycling experiments

It was found that the 3DPNi substrate is suitable for Na metal batteries as well. It showed extremely good Coulombic efficiency for more than 200 cycles with 0.5 $mAh \cdot cm^{-2}$ capacity at a current rate of 1 $mA \cdot cm^{-2}$. However, the voltage hysteresis curves tell us that the Na plating and stripping behaviour is vastly different from the case of Li plating. The potential variations are minimal and the plateaus are more stable. This requires further study as it is clear that the Na cycling behaviour cannot be fully explained by comparison with the Li cycling process.

4.7. Surface layer depositions

ALD of TiO_2 and Al_2O_3 improves the Li cycling performance as expected. The cells show extremely extremely long cycle life of over 300 cycles with very high coulombic efficiency. However, it must be kept in mind that capacity and current rate used here are smaller as compared to the other values. Therefore, the performance of these layers may vary when subjected to higher capacities and current values. Also, it can concluded that the SEI formation mechanism varies in the case - it is visibly slower, especially in the case of Al_2O_3 deposition. This tells us that in the initial cycles, more Li is consumed in the irreversible SEI formation. This is not a detrimental effect in this particular case where we use Li metal as the counter electrode, which provides an unlimited supply of Li. However, in cases where the Li supply is limited (in cells with other electrode materials) this enhanced consumption of Li will lead to rapid capacity loss. Therefore, how the mechanism and dynamics of SEI formation varies with surface layer deposition will be interesting to look into, especially since ALD is a well-developed commercialized technique.

5

Recommendations & Outlook

5.1. Fabrication

There are some limitations to the HBDT method that must be considered. Some of these issues are:

1. The use of extremely high current for the electrodeposition restricts the size of the substrate. The porosity of the substrate depends on the current density of deposition. Hence, to obtain high porosity high current densities are required. The electrodeposition for this work was done at 3 $A{\cdot}cm^{-2}$. So, in order to double the area of deposition we would need to go up to 6 $A{\cdot}cm^{-2}$ which might not be practically viable.
2. The dynamics and chemistry of the HBDT method needs to be studied further. Even though it is a galvanostatic process, the electrochemically active area of the working electrode changes rapidly due to the growth of 3D deposits. Hence, the growth rate - current density relation should be studied further so as to create substrates with desired thickness. Similarly, other parameters like electrolyte composition also plays a significant role in deciding the characteristics of the final deposit.
3. A standardized experimental setup is required to ensure that the substrates with similar, structure and morphology may be created repeatedly. In this work, the entire fabrication work - electrolyte and electrode preparation, deposition and processing was done manually. This could lead to variations among the different samples which could adversely affect the subsequent experiments.
4. The mechanical stability is inversely affected by the porosity. As the porosity of the sample increase, the walls of the 3D network become thinner and weaken the structure. However, there are many ways to improve and modify the structure and porosity of the electrodeposited 3DPNi structure. Post-electrodeposition treatment is a probable option.[61]. In this method, a thin layer of Ni is deposited on the already formed 3DPNi structutre at very low current density ($\sim$ 0.01 $A{\cdot}cm^{-2}$. The low current density ensures that the subsequent Ni deposition happens in a slow and smooth manner. The figure below illustrates the difference in the substrates fabricated with post-electrodeposition. It can be seen that the surface roughness of the sample has reduced significantly as a result of the post-electrodeposition.

5.2. Symmetric cells

The symmetric cells used for this work were lab developed prototype cells. After extended use over long periods of time, the cells have developed minor defects which compromises the performance of some cells and yields faulty results.

An important parameter which affects the process of Li (or Na) cycling is the pressure between the two electrodes inside the cell. In the kind of cells used for this work, the steel spring attached to the flange determines the pressure with which the electrodes are compressed and brought into contact with each other. The tension in the spring show minor variations across the different cells. This leads to electrodes being pressed against each other at different pressures for different cells. The same argument could also be extended to the rubber o-ring. Hence, the reproducibility of results could be an issue and multiple trials with the same experimental settings are advised before the final conclusions are made.

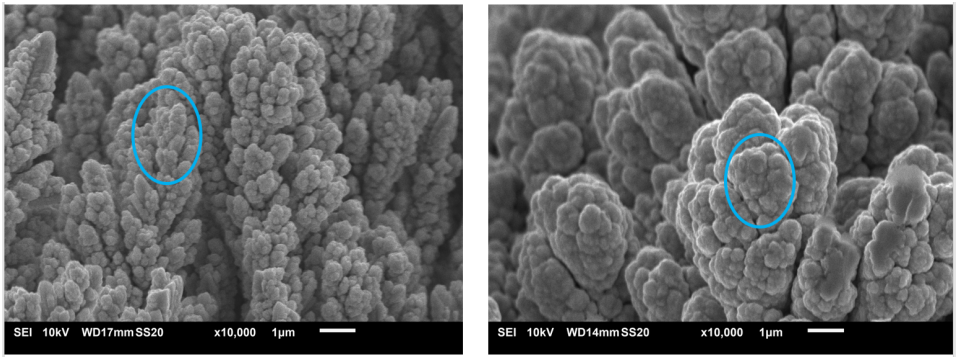

Figure 5.1: Post-electrodeposition effects on the substrate. (a) Normal electrodeposition - grain sizes are smaller as indicated in the highlighted part and (b) Substrate with post-electrodeposition treatment - the highlighted portion shows the reduction in roughness and the grains becoming bigger.

5.3. Li cycling experiments

There are some factors that must be considered while the cycling experiments are performed. They can be summarized as follows:

1. The 3DPNi substrate can be optimized for the Li cycling process. The experiments show that the substrate fabricated with different electrodeposition conditions give us varying Li cycling performance. So, it may be concluded that by individually studying the different properties of the the substrate with respect to its Li cycling performance, we can develop an optimized structure with superior Li cycling performance.
2. The dynamics of SEI formation on a 3D structure needs to be studied further. The SEI formation on a planar structure can be explained by the standard mechanism. However, the SEI formation on a 3D porous structure will also depend on the accessibility of the micro and nano sized pores to the electrolyte. Hence, the SEI formation may not be straightforward and it requires more study.
3. The capacity of Li cycling (and the current rate) and the thickness of substrate are correlated. The cycling performance of the the same substrate might be different for different capacities. Consider the scenario where 0.5 $mAh \cdot cm^{-2}$ of Li is deposited on a substrate fabricated with 60s deposition. If this capacity of Li deposited is lower than the optimal capacity (to contain Li) of the 60s substrate it will result in increased diffusion distances and higher impedance for Li^{+} flow as it moves through the thicker deposit. A probable way to study this could be studying the Li growth/deposition rate on the substrate.

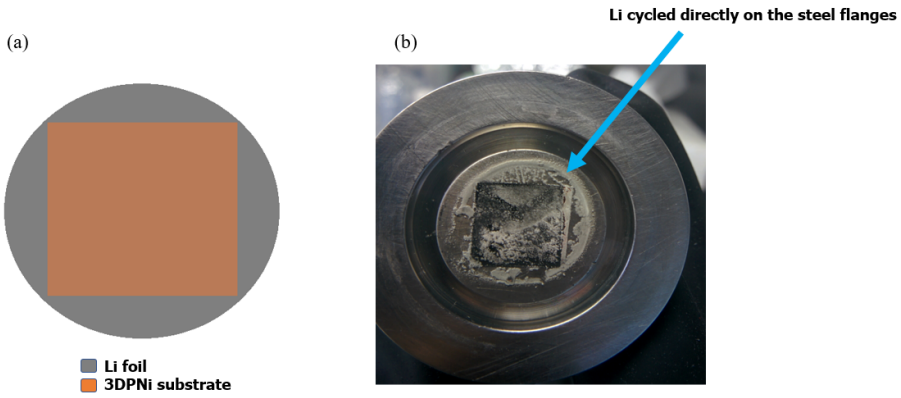

Figure 5.2: Size effects of the electrode. (a) Size variation of the electrodes and (b) Li cycled on the steel flanges.

4. There are some common parameters that influence the Li cycling process in every symmetric cell : capacity, current rate, cut-off voltage for charging and electrode size. The final performance

of the cell is dependent on each of these parameters. Untangling the individual effects of these parameters can help a lot in developing our understanding of the Li cycling performance of the substrate. During the experiments, it was found that the electrodes (Li metal foil and 3DPNi substrate) with similar shape and size can lead to visibly better performance. This is due to the fact using a circular Li foil with 15 mm diameter and a 3DPNi substrate of 1 cm^2 leads to a mismatch in area and this will cause some of the Li to directly cycle with the steel flanges. This especially visible at high capacity cycling and will lead to rapid cell failure. This is shown in the figure below.

Thus, it can be concluded that while gauging the Li cycling performance of the 3DPNi substrate (or any other substrate), the effect of the above-mentioned parameters must be carefully considered while performing the experiments. Only then can we have an effective comparison between the various results published in the scientific literature.

5.4. Full-cell performance

The 3DPNi substrate with pre-deposited Li or Na may be used in full-cells to understand its performance versus other electrode materials. As an example, Li deposited 3DPNi may be cycled with other commercial electrode materials like lithium titanate ($Li_4Ti_5O_{12}$) or lithium iron phosphate ($LiFePO_4$). This will aid in understanding the possibility of commercializing the 3DPNi substrate in the future.

5.5. Standard testing procedure

The comparison between different publications will be effective only if a standardized testing procedure is developed. Hence, developing a standard testing protocol that may be used by research groups all over the world can help in understanding the results as well as gauging other aspects of performance of the system.

A

Appendix

A.1. Materials

The following chemicals were used for this project:

1. Fabrication of 3DPNi
    - $NiSO_4.6/7-H_2O$ - Nickel(II) sulphate hexa-/ heptahydrate - Sigma Aldrich (for nickel plating, DIN 50970 H, ≥20.6% Ni and Co basis)
    - NH_4Cl - Ammonium chloride - Sigma Aldrich (puriss. p.a., ACS reagent, reag. ISO, reag. Ph. Eur., ≥99.5%)
    - PEG4000 - Poly(ethylene glycol) - Sigma Aldrich (average Mn 4,000, platelets)
2. Electrolytes
    - LiTFSI - Bis(trifluoromethane)sulfonimide lithium salt - Sigma Aldrich (CAS Number 90076-65-6)
    - DME - 1,2 Dimethoxyethane - Sigma Aldrich (anhydrous, 99.5%, inhibitor-free)
    - DOL - 1,3 Dioxolane - Sigma Aldrich (anhydrous, contains 75 ppm BHT as inhibitor, 99.8
    - $LiNO_3$ - Lithium nitrate - (99.99% trace metals basis)
    - $NaPF_6$ - Sodium hexafluorophosphate - Sigma Aldrich (98%)
    - DEGDME - Diethylene glycol dimethyl ether - Sigma Aldrich (anhydrous, 99.5%)

A.2. Maccor test system & Failure modes

A.2.1. Maccor test system

The Li and Na cycling done in this work were carried out by the Maccor system. The data was analyzed by the MIMS client software. The test procedure for the cell is fed to the software before the cycling process has started. The results screen of the Maccor program with the software looks like this,

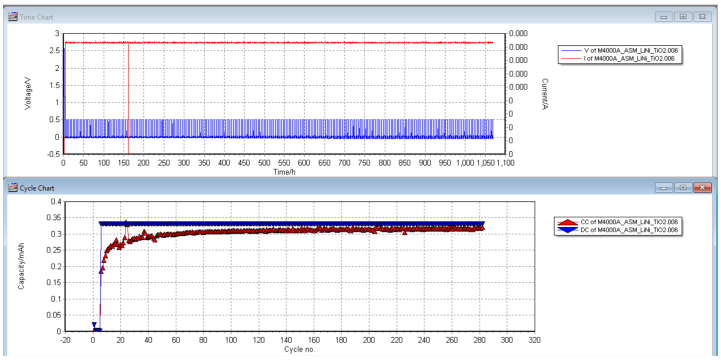

Figure A.1: Output data screen of the Li cycling process with Maccor.

The screen is divided into two plots. The plot on the top shows the voltage profile (voltage vs. time) of the process. The plot at the bottom shows the discharge and charge capacity vs. the cycle number of the cycling process. Both the graphs together tell us how the cycling is progressing.

A.2.2. Failure Modes

Figure A.1 is a cell that has performed well for over 300 cycles. As is clear from the image, the voltage profile is extremely stable and the Coulombic efficiency is does not fluctuate haphazardly, maintaining a value of more than 90% once the cell is stabilized. Comparing figure A.1 to the figure below (A.2) shows a clear distinction between a working and failed cell.

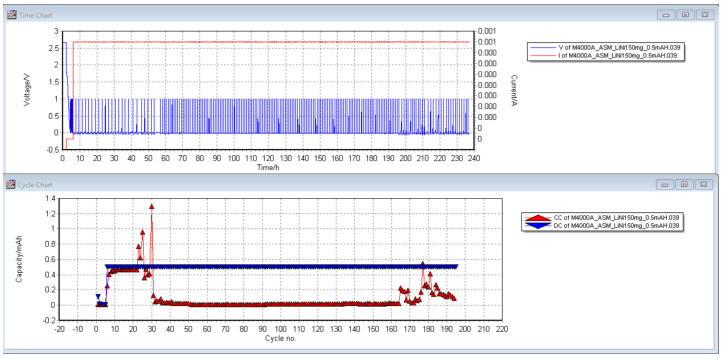

Figure A.2: Output data screen of the Li cycling process with Maccor - Failed cell

It is evident from the picture that the voltage profile has destabilized and is at 0 V (i.e short-circuit) from about 60 hours. This correspondingly reflected in the charge-discharge capacity curves as well. The charging capacity drops to zero which means that the cycling process has stopped and there is no stripping happening. Li plating happens as per the program, but the cell is unable to support the stripping process.

By disassembling a cell in the glovebox, we can see some of the problems that happen during the preparation of the cell, as well as during the cycling process.

Figure A.3: Fresh Li (inset) compared to the one after cycling. The black particles on the surface are the dendrites.

The black powdery deposits at the surface of the Li metal is the dendrites formed. Proper cell assembly is crucial to the successful cyling of the cell. The images below show the most common ways that cell assembly and cycling may go wrong.

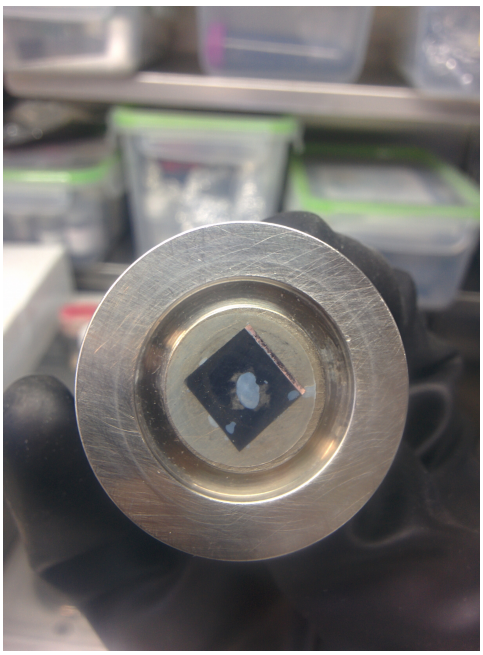

Figure A.4: The separator was not placed properly on the 3DPNi substrate. The gas bubble trapped under it can be seen clearly.

Figure A.5: Comparison of 3mAh·cm^{-2} of Li deposited on the 3DPNi (left) and Cu (right) substrate. The homogeneity in the case of 3DPNi is evident.

Bibliography

[1] J.-K. Park, *Principles and applications of lithium secondary batteries* (John Wiley & Sons, 2012).

[2] *Global EV Outlook 2016 : Beyond one million electric cars* (International Energy Agency, 2016).

[3] D. Lin, Y. Liu, and Y. Cui, *Reviving the lithium metal anode for high-energy batteries,* Nature Nanotechnology **12**, 194 (2017).

[4] Z. W. Seh, J. Sun, Y. Sun, and Y. Cui, *A highly reversible room-temperature sodium metal anode,* ACS central science **1**, 449 (2015).

[5] D. Howell, B. Cunningham, T. Duong, and P. Faguy, *Overview of the doe vto advanced battery r&d program,* Annual Merit Review June **6** (2016).

[6] P. Roy and S. K. Srivastava, *Nanostructured anode materials for lithium ion batteries,* Journal of Materials Chemistry A **3**, 2454 (2015).

[7] M. Sathiya, G. Rousse, K. Ramesha, C. Laisa, H. Vezin, M. T. Sougrati, M.-L. Doublet, D. Foix, D. Gonbeau, W. Walker, *et al.*, *Reversible anionic redox chemistry in high-capacity layered-oxide electrodes,* Nature materials **12**, 827 (2013).

[8] J. Christensen, P. Albertus, R. S. Sanchez-Carrera, T. Lohmann, B. Kozinsky, R. Liedtke, J. Ahmed, and A. Kojic, *A critical review of li/air batteries,* Journal of the Electrochemical Society **159**, R1 (2011).

[9] Y.-X. Yin, S. Xin, Y.-G. Guo, and L.-J. Wan, *Lithium–sulfur batteries: electrochemistry, materials, and prospects,* Angewandte Chemie International Edition **52**, 13186 (2013).

[10] C. J. Orendorff, *The role of separators in lithium-ion cell safety,* The Electrochemical society interface **21**, 61 (2012).

[11] A. H. Whitehead and M. Schreiber, *Current collectors for positive electrodes of lithium-based batteries,* Journal of The Electrochemical Society **152**, A2105 (2005).

[12] D. W. I. R. M. Hahn, *Techniques for raman analysis of lithium-ion batteries,* (2015).

[13] M. S. Park, S. B. Ma, D. J. Lee, D. Im, S.-G. Doo, and O. Yamamoto, *A highly reversible lithium metal anode,* Scientific reports **4**, 3815 (2014).

[14] J. B. Goodenough, *Energy storage materials: a perspective,* Energy Storage Materials **1**, 158 (2015).

[15] E. C. Evarts, *Lithium batteries: To the limits of lithium,* Nature **526**, S93 (2015).

[16] J. Lang, L. Qi, Y. Luo, and H. Wu, *High performance lithium metal anode: Progress and prospects,* Energy Storage Materials (2017).

[17] G. Girishkumar, B. McCloskey, A. Luntz, S. Swanson, and W. Wilcke, *Lithium- air battery: promise and challenges,* The Journal of Physical Chemistry Letters **1**, 2193 (2010).

[18] M. Zier, F. Scheiba, S. Oswald, J. Thomas, D. Goers, T. Scherer, M. Klose, H. Ehrenberg, and J. Eckert, *Lithium dendrite and solid electrolyte interphase investigation using oso 4,* Journal of Power Sources **266**, 198 (2014).

[19] X.-B. Cheng, R. Zhang, C.-Z. Zhao, F. Wei, J.-G. Zhang, and Q. Zhang, *A review of solid electrolyte interphases on lithium metal anode,* Advanced Science **3** (2016).

[20] W. Xu, J. Wang, F. Ding, X. Chen, E. Nasybulin, Y. Zhang, and J.-G. Zhang, *Lithium metal anodes for rechargeable batteries,* Energy & Environmental Science **7**, 513 (2014).

[21] Z. Li, J. Huang, B. Y. Liaw, V. Metzler, and J. Zhang, *A review of lithium deposition in lithium-ion and lithium metal secondary batteries,* Journal of power sources **254**, 168 (2014).

[22] L. Gireaud, S. Grugeon, S. Laruelle, B. Yrieix, and J.-M. Tarascon, *Lithium metal stripping/plating mechanisms studies: A metallurgical approach,* Electrochemistry communications **8**, 1639 (2006).

[23] K. N. Wood, M. Noked, and N. P. Dasgupta, *Lithium metal anodes: toward an improved understanding of coupled morphological, electrochemical, and mechanical behavior,* ACS Energy Letters **2**, 664 (2017).

[24] K. J. Harry, D. T. Hallinan, D. Y. Parkinson, A. A. MacDowell, and N. P. Balsara, *Detection of subsurface structures underneath dendrites formed on cycled lithium metal electrodes,* Nature materials **13**, 69 (2014).

[25] J.-N. Chazalviel, *Electrochemical aspects of the generation of ramified metallic electrodeposits,* Physical review A **42**, 7355 (1990).

[26] D. Wang, W. Zhang, W. Zheng, X. Cui, T. Rojo, and Q. Zhang, *Towards high-safe lithium metal anodes: Suppressing lithium dendrites via tuning surface energy,* Advanced Science **4** (2017).

[27] V. Palomares, P. Serras, I. Villaluenga, K. B. Hueso, J. Carretero-González, and T. Rojo, *Na-ion batteries, recent advances and present challenges to become low cost energy storage systems,* Energy & Environmental Science **5**, 5884 (2012).

[28] S. Shiraishi, K. Kanamura, and Z.-i. Takehara, *Surface condition changes in lithium metal deposited in nonaqueous electrolyte containing hf by dissolution-deposition cycles,* Journal of The Electrochemical Society **146**, 1633 (1999).

[29] W. Li, H. Yao, K. Yan, G. Zheng, Z. Liang, Y.-M. Chiang, and Y. Cui, *The synergetic effect of lithium polysulfide and lithium nitrate to prevent lithium dendrite growth,* Nature communications **6** (2015).

[30] F. Ding, W. Xu, G. L. Graff, J. Zhang, M. L. Sushko, X. Chen, Y. Shao, M. H. Engelhard, Z. Nie, J. Xiao, *et al.*, *Dendrite-free lithium deposition via self-healing electrostatic shield mechanism,* Journal of the American Chemical Society **135**, 4450 (2013).

[31] R. Kanno and M. Murayama, *Lithium ionic conductor thio-lisicon: The li2 s ges2 p 2 s 5 system,* Journal of The Electrochemical Society **148**, A742 (2001).

[32] Y. Inaguma, C. Liquan, M. Itoh, T. Nakamura, T. Uchida, H. Ikuta, and M. Wakihara, *High ionic conductivity in lithium lanthanum titanate,* Solid State Communications **86**, 689 (1993).

[33] U. v. Alpen, A. Rabenau, and G. Talat, *Ionic conductivity in li3n single crystals,* Applied Physics Letters **30**, 621 (1977).

[34] H. Aono, E. Sugimoto, Y. Sadaoka, N. Imanaka, and G.-y. Adachi, *Ionic conductivity of solid electrolytes based on lithium titanium phosphate,* Journal of the electrochemical society **137**, 1023 (1990).

[35] F. Croce, G. Appetecchi, L. Persi, and B. Scrosati, *Nanocomposite polymer electrolytes for lithium batteries,* Nature **394**, 456 (1998).

[36] G. A. Umeda, E. Menke, M. Richard, K. L. Stamm, F. Wudl, and B. Dunn, *Protection of lithium metal surfaces using tetraethoxysilane,* Journal of Materials Chemistry **21**, 1593 (2011).

[37] N.-W. Li, Y.-X. Yin, C.-P. Yang, and Y.-G. Guo, *An artificial solid electrolyte interphase layer for stable lithium metal anodes,* Advanced Materials (2015).

[38] G. Zheng, S. W. Lee, Z. Liang, H.-W. Lee, K. Yan, H. Yao, H. Wang, W. Li, S. Chu, and Y. Cui, *Interconnected hollow carbon nanospheres for stable lithium metal anodes,* Nature nanotechnology **9**, 618 (2014).

[39] J.-S. Kim, D. W. Kim, H. T. Jung, and J. W. Choi, *Controlled lithium dendrite growth by a synergistic effect of multilayered graphene coating and an electrolyte additive,* Chemistry of Materials **27**, 2780 (2015).

[40] C.-P. Yang, Y.-X. Yin, S.-F. Zhang, N.-W. Li, and Y.-G. Guo, *Accommodating lithium into 3d current collectors with a submicron skeleton towards long-life lithium metal anodes,* Nature communications **6**, 8058 (2015).

[41] Z. Liang, G. Zheng, C. Liu, N. Liu, W. Li, K. Yan, H. Yao, P.-C. Hsu, S. Chu, and Y. Cui, *Polymer nanofiber-guided uniform lithium deposition for battery electrodes,* Nano letters **15**, 2910 (2015).

[42] D. Lin, Y. Liu, Z. Liang, H.-W. Lee, J. Sun, H. Wang, K. Yan, J. Xie, and Y. Cui, *Layered reduced graphene oxide with nanoscale interlayer gaps as a stable host for lithium metal anodes,* Nature nanotechnology **11**, 626 (2016).

[43] Y. Liu, D. Lin, Z. Liang, J. Zhao, K. Yan, and Y. Cui, *Lithium-coated polymeric matrix as a minimum volume-change and dendrite-free lithium metal anode,* Nature communications **7** (2016).

[44] K. Yan, Z. Lu, H.-W. Lee, F. Xiong, P.-C. Hsu, Y. Li, J. Zhao, S. Chu, and Y. Cui, *Selective deposition and stable encapsulation of lithium through heterogeneous seeded growth,* Nature Energy **1**, 16010 (2016).

[45] B. J. Plowman, L. A. Jones, and S. K. Bhargava, *Building with bubbles: the formation of high surface area honeycomb-like films via hydrogen bubble templated electrodeposition,* Chemical Communications **51**, 4331 (2015).

[46] C. Marozzi and A. Chialvo, *Development of electrode morphologies of interest in electrocatalysis. part 1: Electrodeposited porous nickel electrodes,* Electrochimica Acta **45**, 2111 (2000).

[47] C. Marozzi and A. Chialvo, *Development of electrode morphologies of interest in electrocatalysis: part 2: hydrogen evolution reaction on macroporous nickel electrodes,* Electrochimica acta **46**, 861 (2001).

[48] K. Tan, M.-B. Tian, and Q. Cai, *Effect of bromide ions and polyethylene glycol on morphological control of electrodeposited copper foam,* Thin Solid Films **518**, 5159 (2010).

[49] C. Grey and J. Tarascon, *Sustainability and in situ monitoring in battery development,* Nature materials **16**, 45 (2017).

[50] Y.-J. Kim, H. Lee, H. Noh, J. Lee, S. Kim, M.-H. Ryou, Y. M. Lee, and H.-T. Kim, *Enhancing the cycling stability of sodium metal electrodes by building an inorganic–organic composite protective layer,* ACS applied materials & interfaces **9**, 6000 (2017).

[51] A. C. Kozen, C.-F. Lin, A. J. Pearse, M. A. Schroeder, X. Han, L. Hu, S.-B. Lee, G. W. Rubloff, and M. Noked, *Next-generation lithium metal anode engineering via atomic layer deposition,* ACS nano **9**, 5884 (2015).

[52] Y. Xu, E. Swaans, S. Chen, S. Basak, P.-P. R. Harks, B. Peng, H. W. Zandbergen, D. M. Borsa, and F. M. Mulder, *A high-performance li-ion anode from direct deposition of si nanoparticles,* Nano Energy (2017).

[53] M. S. 4000, *http://www.maccor.com/products/series4000.aspx,* (2017-07-04).

[54] B. of Electrochemical Impedance Spectroscopy, *https://www.gamry.com/application-notes/eis/basics-of-electrochemical-impedance-spectroscopy/,* (2017-07-03).

[55] S. I. to Analyze the Li-Ion Battery with an App, *https://www.comsol.com/blogs/studying-impedance-to-analyze-the-li-ion-battery-with-an-app/,* (2017-07-03).

[56] N. Sekar and R. P. Ramasamy, *Electrochemical impedance spectroscopy for microbial fuel cell characterization,* J Microb Biochem Technol S **6** (2013).

[57] I. Rose and C. Whittington, *Nickel plating handbook,* .

[58] X. Guo, X. Li, Y. Zheng, C. Lai, W. Li, B. Luo, and D. Zhang, *Effects of surfactants on high regularity of 3d porous nickel for zn2,* Journal of Nanomaterials **2014** (2014).

[59] A. Pei, G. Zheng, F. Shi, Y. Li, and Y. Cui, *Nanoscale nucleation and growth of electrodeposited lithium metal,* Nano letters **17**, 1132 (2017).

[60] D. Aurbach, E. Pollak, R. Elazari, G. Salitra, C. S. Kelley, and J. Affinito, *On the surface chemical aspects of very high energy density, rechargeable li–sulfur batteries,* Journal of The Electrochemical Society **156**, A694 (2009).

[61] R. Kim, D. Han, D. Nam, J. Kim, and H. Kwon, *Effects of substrate morphology and postelectrodeposition on structure of cu foam and their application for li-ion batteries,* Journal of The Electrochemical Society **157**, D269 (2010).